https://doi.org/10.1016/j.applthermaleng.2018.10.073


# Mathematical modeling of direct ethylene glycol fuel cells incorporating the effect of the competitive adsorption

Zhefei Pan[1], Yanding Bi[1], Liang An*

Department of Mechanical Engineering, The Hong Kong Polytechnic University, Hung Hom, Kowloon, Hong Kong SAR, China

[1] Equal contribution.

*Corresponding author.

Email: liang.an@polyu.edu.hk (L. An)

## Abstract

In this work, a one-dimensional mathematical model for a direct ethylene glycol fuel cell using hydrogen peroxide as oxidant is developed. This model considers the ethylene glycol crossover and the competitive adsorption between ethylene glycol molecules and hydroxyl ions at reaction sites, in addition to mass/charge transport and electrochemical reactions. In addition, the complicated co-existence of the hydrogen peroxide reduction reaction, the hydrogen peroxide oxidation reaction, and the oxygen reduction reaction in the cathode is also considered in this model. The mathematical model under the consideration of the above-mentioned physicochemical processes exhibits a good agreement with experimental results. In addition, the effects of various operating and electrode structural parameters on the cell performance are examined, including concentrations of various species, the exchange current density and the thickness of diffusion layer. The numerical results exhibit that the cell performance improves with the increasing concentrations of hydrogen peroxide and sulfuric acid. As for the ethylene glycol and hydroxyl ions, increasing the concentrations makes contribution to higher

performance, while the cell performance experiences a degradation at a high current density region due to the remarkable ohmic loss. The model also shows that increasing both the anode and cathode exchange current density leads to an improved cell performance, which indicates the significance of developing novel catalyst with superior catalytic activity. Moreover, the effect of the structural design parameters of the anode and cathode diffusion layer is also investigated, and the results show that increasing thickness of diffusion layers has a negative effect on the cell performance.

**Keywords:** Direct ethylene glycol fuel cell; Hydrogen peroxide; Mathematical modeling; Mass transport; Competitive adsorption; Fuel crossover

## 1. Introduction

Direct alcohol fuel cells (DAFCs) have received ever-increasing attention as a propitious power source, primarily due to their high efficiency, simple design, quick refueling as well as low emissions [1-5]. Among various alcohol fuels, small molecule and short-chain alcohols, e.g., methanol and ethanol, are regarded as promising fuel candidates, because the rate of oxidation reaction is higher than that of large molecule and long-chain alcohols [6-9]. Although promising, direct methanol fuel cells (DMFCs) suffer from the severe performance decline derived from the serious methanol crossover and poisonousness of derivative to the catalyst [6]. In addition, direct ethanol fuel cells (DEFCs) exhibit a low electron transfer rate (33%) due to the hardly broken C-C bond at low temperatures (generally < 60$^{o}$C) [10, 11]. Recently, direct ethylene glycol fuel cells (DEGFCs) running on ethylene glycol (EG), which are regarded as an alternative DAFC, have attracted great attention for mobile, stationary, and portable applications, which is attributed to its intrinsic superiorities, including high theoretical energy capacity (4.8 Ah $mL^{-1}$), high boiling point (198$^{o}$C), and high electron transfer rate (80%) [12-16]. In addition, using hydrogen peroxide as oxidant in the cathode to replace the air or pure oxygen has been extensively studied [17-19]. The use of liquid hydrogen peroxide brings about the following advantages: (1) a substantial increase in the theoretical voltage; (2) low activation loss of the reduction reaction due to two-electron transfer; and (3) no water flooding problem [20]. Moreover, hydrogen peroxide is more favorable in air shortage situations, e.g., outer space and underwater. For instance, Pan et al. [19] developed a hybrid DEGFC using hydrogen peroxide as oxidant yielding an open-circuit voltage (OCV) of 1.41 V and a peak power density of 80.9 mW $cm^{-2}$ at 60°C. It was reported that the hybrid DEGFC boosted the OCV by 62.1% and the peak power density by 20.8% comparing to the same cell using oxygen.

In general, the fuel cell performance relies on various parameters, including the materials and electrode structures, species concentrations, as well as operating temperature [21-23]. However, investigating the effect of each parameter on cell performance via experimental approach is quite cost-ineffective and time-consuming. Thus, mathematical modeling, which is regarded as an economical and powerful tool, is essential for the detailed study and optimization of operating parameters of fuel cells, so that the performance can be maximized [24]. Jiao et al. [25] presented an excellent work on water transport in polymer electrolyte membrane fuel cells (PEMFCs) and comprehensively reviewed different models adopted for different purposes in water transport in PEMFCs. Bahrami et al. [26] proposed a one-dimensional, isothermal, single-phase model to investigate the mass transport in a DEFC, but the addition of alkali was not taken into consideration. Recently, Guo et al. [27] developed a transient two-dimensional multi-phase model for passive vapor-feed DMFC fed with neat methanol to investigate the mass transport processes with different cell designs and operation conditions. Xie et al. [28] further studied the effects of open ratio, carbon dioxide exit length, micro-porous layer (MPL) and porous layer's hydrophobicity on the cell performance. Wang et al. [29] developed a quasi-2D transient model of proton exchange membrane fuel cell with anode recirculation. Huo et al. [30] investigated the effect of various operating pressures on the water transfer mechanism in an alkaline electrolyte membrane fuel cell and studied the effect of operating behavior on the cell performance both experimentally test and analytically.

It should be mentioned that the addition of alkali in the anode can improve the electrochemical kinetics of the EG oxidation reaction (EGOR), but the anode becomes a complex cation-anion co-existing compartment, which makes the physicochemical processes in the fuel cell system more complicated, including mass transport, electron transport, ion transport, as well as

electrochemical reactions [31]. Meanwhile, the involvement of hydrogen peroxide and acid in the cathode also entangles the physicochemical processes. On one hand, the mass transport, electron transport, and ion transport are more convoluted, which is similar to the situation in the anode. On the other hand, not only the hydrogen peroxide reduction reaction (HPRR) takes place in the cathode, but the hydrogen peroxide oxidation reaction (HPOR) also occurs simultaneously. Moreover, the oxygen derived from the HPOR also can participate in reduction reactions. Therefore, there are two reduction reactions and an oxidation reaction existing in the cathode, which may spontaneously establish an internal hydrogen peroxide fuel cell. To our best knowledge, there is no attempt to mathematically investigate the alkaline DEGFC with hydrogen peroxide as oxidant. In this work, a comprehensive one-dimensional steady-state isothermal mathematical model is developed to extensively investigate the operating parameters and electrode designs on the cell performance.

## 2. Formulation

As depicted in Figure 1, the DEGFC consists of the anode/cathode flow fields (FFs), the anode/cathode diffusion layers (DLs), the anode/cathode catalyst layers (CLs), and a cation exchange membrane (CEM). In the anode, the anolyte containing EG and NaOH transports from the anode FF through the anode DL to the anode CL, where the EG reacts with hydroxyl ions to produce electrons, oxalate and water. The EGOR reaction is shown as follows [11]:

$$C_2H_6O_2+10OH^-\rightarrow(COO^-)_2+8e^-+8H_2O \qquad E_{EGOR}=-0.69\ V \qquad (1)$$

The electrons produced on the anode are transported through the external circuit to the cathode, where the HPRR occurs according to [32]:

$$4H_2O_2+8H^++8e^-\rightarrow8H_2O \qquad E_{HPRR}=1.78\ V \qquad (2)$$

Meanwhile, the sodium ions are transported from the anode to cathode through the membrane, which forms the internal ionic circuit. Consequently, the overall reaction of the passive DEGFC can be obtained by combining EGOR on the anode and HPRR on the cathode as follows:

$$C_2H_6O_2+4H_2O_2+8H^++10OH^-\rightarrow(COO^-)_2+16H_2O \quad E=2.47\ V \tag{3}$$

In the present work, the model equations are defined in one direction (x-axis) through the anode, CEM, and cathode. To simplify the complicated processes, the following assumptions and simplifications are made:

(1) The fuel cell is assumed to operate under steady-state and isothermal conditions.

(2) The mass/charge transport through the cathode DL is assumed to be a diffusion-predominated process, while both diffusion and convection are considered in the anode DL.

(3) The CLs are too thin so that they are treated as interfaces.

(4) The competitive adsorption on the active sites is assumed to be concentration-dependent.

(5) The EG transporting through the membrane is completely oxidized in the cathode so that the EG concentration in cathode CL is zero.

(6) The hydroxyl-ion crossover, hydrogen peroxide crossover, and oxygen crossover through the membrane are ignored.

### 2.1. Anode

#### 2.1.1. Mass transport

In the anode DL, where no chemical reaction occurs, the species flux ($N_i^{\mathrm{ADL}}$) remains constant. The flux expression is developed based on the work of Pathak and Basu [33] and can be presented as:

$$N_i^{ADL}=\frac{C_i^F e^{v^{ADL}/k_i^{ADL}}-C_i^{ACL}}{e^{v^{ADL}/k_i^{ADL}}-1}v^{ADL} \tag{4}$$

where $C_i^F$ is the feeding concentration ($i$: EG, $OH^-$), $v^{ADL} = k_w \Delta P/\mu_w l_{ADL}$ is the superficial velocity of water in the anode DL, $k_i^{ADL} = D_i^{ADL,eff}/l_d$ is the mass transfer coefficient in the anode DL, and $C^{ACL}$ is the species concentration in the anode CL. The $D_i^{eff}$ is given by [34]:

$$D_i^{eff} = \varepsilon^{3/2} D_i \tag{5}$$

where $\varepsilon$ is the porosity of the anode DL, and the $D_i$ is free-space diffusivity of species ($i$: EG, $OH^-$). In the anode CL, since the mass transport is considered to be diffusion-predominated, the flux ($N_i^S$) can be obtained based on Fick's law:

$$N_i^S = -D_i^{eff} \frac{C_i^{ACL} - C_i^S}{\delta_{ACL}} \tag{6}$$

where $C_i^{ACL}$ is the species concentration in the anode CL, the $C_i^s$ is the species concentration on the catalyst, and $\delta_{ACL}$ is the radius of the bulk. Through the membrane, the EG crossover ($N_i^M$) is in the same way as it transports through DL. Hence, it is given by:

$$N_i^M = \frac{C_i^{ACL} e^{v^M/k^M}}{e^{v^M/k^M} - 1} v^M \tag{7}$$

where $v^M = k_w \Delta P/\mu_w l_M$ is the superficial velocity of water in membrane, $k^M = D^{M,eff}/l_M$ is the mass transfer coefficient in membrane. It is believed that the electrochemical reactions take place at the active sites on the catalyst, which implies that the actual reactant concentration participating in the EGOR does not equal to the species concentration on the catalyst surface. In other words, for a specific active site, the actual reactant concentration mainly depending on the species concentration on the catalyst surface is the result of the competitive adsorption between EG and $OH^-$. It is clear that the reactant with higher concentration is more likely to be adsorbed on the active sites, thus the assumption that the competitive adsorption on the active sites is concentration-dependent is made. Based on this assumption, the actual reactant concentration can be given by:

$$C_{EG}^{R} = \frac{C_{EG}^{S}}{C_{EG}^{S}+C_{OH^-}^{S}} C_{EG}^{S} \quad (8)$$

$$C_{OH^-}^{R} = \frac{C_{OH^-}^{S}}{C_{EG}^{S}+C_{OH^-}^{S}} C_{OH^-}^{S} \quad (9)$$

where $C_i^R$ is the actual reactant concentration at the active sites (*i: EG, OH*$^-$), and $C_i^S$ is the reactant concentration on the catalyst surface.

### 2.1.2. Electrochemical kinetics

The EGOR is a multi-step and multi-pathway electrochemical process; therefore, its reaction mechanism has not been completely understood yet. Herein, a Tafel-form electrochemical model for the EGOR incorporating the mass transport effect is adopted:

$$j_a = i_{0,a}\left(\frac{C_{EG}^{R}}{C_{EG}^{ref}}\right)^{\gamma_a^{EG}}\left(\frac{C_{OH^-}^{R}}{C_{OH^-}^{ref}}\right)^{\gamma_a^{OH^-}} \exp\left(\frac{\alpha_a F}{RT}\eta_a\right) \quad (10)$$

$$\gamma_a^{EG}\begin{cases} 0 & C_{EG}^{R} > C_{EG}^{ref} \\ 1 & C_{EG}^{R} \le C_{EG}^{ref} \end{cases} \quad (11)$$

$$\gamma_a^{OH^-}\begin{cases} 0 & C_{OH^-}^{R} > C_{OH^-}^{ref} \\ 1 & C_{OH^-}^{R} \le C_{OH^-}^{ref} \end{cases} \quad (12)$$

where $C_i^R$ is the reactant concentration on the active sites, $C_i^{\mathrm{ref}}$ is the reference reactant concentration, and $\gamma$ is the reaction order related to the species concentration. When the concentration is higher than a reference value, it is zero. Otherwise, it is one.

## 2.2. Cathode

In the cathode, the formation for the mass/charge transport and electrochemical reactions is based on our previous work [17]. Briefly, the species flux in the cathode DL ($N_i^{\mathrm{CDL}}$) can be described according to:

$$N_i^{CDL} = -D_i^{eff}\frac{dc_i^F}{dx} \quad (13)$$

where $C_i^F$ is the feeding concentration ($i$: $H_2O_2$, $H^+$). The superficial current density $j_c$ can be defined by three respective current densities, which are $j_{HPRR}$ derived from HPRR, $j_{HPOR}$ derived from HPOR, as well as $j_{ORR}$ derived from oxygen reduction reaction (ORR):

$$
\begin{aligned}
j_c &= j_{HPRR} + j_{ORR} - j_{HPOR} \\
&= i_{0,HPRR}\left(\frac{C_{H_2O_2}^{CL}}{C_{H_2O_2}^{ref}}\right)^{\gamma_{HPRR}^{H_2O_2}}\left(\frac{C_{H^+}^{CL}}{C_{H^+}^{ref}}\right)^{\gamma_{HPRR}^{H^+}} \exp\left[\frac{\alpha_{HPRR}F}{RT}(E_{HPRR}^0 - E_{mixed})\right] \\
&+ i_{0,ORR}\left(\frac{C_{O_2}^{CL}}{C_{O_2}^{ref}}\right)^{\gamma_{ORR}^{O_2}}\left(\frac{C_{H^+}^{CL}}{C_{H^+}^{ref}}\right)^{\gamma_{ORR}^{H^+}} \exp\left[\frac{\alpha_{ORR}F}{RT}(E_{ORR}^0 - E_{mixed})\right] \\
&- n_{HPOR}Fk\exp[\frac{\alpha_{HPOR}F}{RT}(E_{mixed} - E_{HPOR}^0)]\theta_{H_2O_2}
\end{aligned}
\tag{14}
$$

$$
\gamma_{HPRR}^{H_2O_2}\begin{cases}0 & C_{H_2O_2}^{CL} > C_{H_2O_2}^{ref} \\ 1 & C_{H_2O_2}^{CL} \le C_{H_2O_2}^{ref}\end{cases} \tag{15}
$$

$$
\gamma_{HPRR}^{H^+}\begin{cases}0 & C_{H^+}^{CL} > C_{H^+}^{ref} \\ 1 & C_{H^+}^{CL} \le C_{H^+}^{ref}\end{cases} \tag{16}
$$

$$
\gamma_{ORR}^{O_2}\begin{cases}0 & C_{O_2}^{CL} > C_{O_2}^{ref} \\ 1 & C_{O_2}^{CL} \le C_{O_2}^{ref}\end{cases} \tag{17}
$$

$$
\gamma_{ORR}^{H^+}\begin{cases}0 & C_{H^+}^{CL} > C_{H^+}^{ref} \\ 1 & C_{H^+}^{CL} \le C_{H^+}^{ref}\end{cases} \tag{18}
$$

where $i_{0,HPRR}$ is the exchange current density of HPRR, $i_{0,ORR}$ is the exchange current density of ORR, $C_i^{CL}$ is the reactant concentration on the cathode CL, $C_i^{ref}$ is the reference reactant concentration, $\gamma$ is the reaction order based on the concentration of different species, $E^0$ is the theoretical potential, $k$ is the rate constant, $\alpha$ is the transfer coefficient, $\theta_{H_2O_2}$ is the coverage of $H_2O_2$ on the catalyst, $E_{mixed}$ is the mixed potential.

### 2.3. Boundary conditions

In the anode,

$x = x_1$: $C_i = C_i^F$ ($i$: EG, $OH^-$) (19)

$x = x_2$: $N_i^S = \frac{i_{cell} S_i}{n_a F}$ ($i$: EG, $OH^-$) (20)

Through the membrane,

$x = x_3$: $C_{i,\,x3} = c_{i,\,x2}$ ($i$: EG, $OH^-$) (21)

$x = x_4$: $C_{i,\,x4} = 0$ ($i$: EG) (22)

In the cathode,

$x = x_5$: $N_{H_2O_2} = \frac{S_{HPRR}^{H_2O_2} j_{HPRR}}{n_{HPRR} F} + \frac{S_{HPOR}^{H_2O_2} j_{HPOR}}{n_{HPOR} F}$ (23)

$$N_{H^+} = \frac{S_{HPRR}^{H^+} j_{HPRR}}{n_{HPRR} F} + \frac{S_{ORR}^{H^+} j_{ORR}}{n_{ORR} F} - \frac{S_{HPOR}^{H^+} j_{HPOR}}{n_{HPOR} F} \quad (24)$$

$$N_{O_2} = \frac{S_{ORR}^{O_2} j_{ORR}}{n_{ORR} F} - \frac{S_{HPOR}^{O_2} j_{HPOR}}{n_{HPOR} F} \quad (25)$$

$x = x_6$: $C_i = C_i^F$ ($i$: $H_2O_2$, $H^+$) (26)

where $s$ is the stoichiometric coefficient, and $n$ is the number of electrons transferred.

### 2.4. Cell voltage

The cell voltage can be determined by Equation (27):

$$V_{cell} = E_c^0 - E_a^0 - \eta_a - \eta_c - i_{cell} R_{internal} \quad (27)$$

where $\eta_a$ is the anode polarization, $\eta_c$ is the cathode polarization, and $R_{internal}$ is the overall internal resistance, which is measured by experiment. The physicochemical, operating, structural, and transport parameters are shown in Tables 1–4, respectively. In addition, above equations are numerically solved by using Matlab.

### 2.5. Experimental

The home-made fuel cell was composed of a Pd-based anode, a cation exchange membrane, and a gold-based cathode. The anode electrode was prepared by spraying the catalyst ink (1.0 mg $cm^{-2}$ Pd/C and 5 wt. % Nafion) onto a piece of carbon cloth with an active area of 1.0 cm × 1.0 cm. The cathode electrode was made by spraying the catalyst ink (2.66 mg $cm^{-2}$ Au/C and 15 wt. % Nafion) onto a piece of carbon cloth with the same active area. The membrane electrode assembly (MEA) was fixed between an anode plate and a cathode plate, both of which are made of 316 L stainless steel plates with serpentine flow fields. The polarization curves were measured by an Arbin BT2000 (Arbin Instrument Inc.) and the internal resistance was measured by the built-in function of the Arbin BT2000.

## 3. Results and discussion

### 3.1. Model validation

As shown in Figure 2, the comparison between the numerical results of the polarization curves under various EG concentrations, i.e. 0.5 M, 1.0 M, and 2.0 M, and the experimental results are made. The experimental results were obtained with a home-made fuel cell. The experimental results were collected when the home-made cell was running with a mixed solution of 7.0 M NaOH and EG as the fuel and a mixed solution of 4.0 M $H_2O_2$ and 1.0 M $H_2SO_4$ as the oxidant at 60ºC. It is shown that the predicted cell performance is in good agreement with the experimental data. In the following sections, the voltage losses as well as the effects of species concentrations, electrocatalyst activities, and electrode structures on the cell performance will be presented.

### 3.2. Voltage loss

As shown in Figure 3, anode polarization, ohmic polarization, and cathode polarization are demonstrated, all of which result in the voltage loss between the theoretical cell voltage and the practical cell voltage. In general, both the anode and the cathode are suffering from activation

polarization and concentration polarization derived from electrochemical loss and transport loss, respectively [46]. Meanwhile, the ohmic polarization derived from internal resistance also occurs. It is seen that the cathode polarization is the severest voltage loss among the anode polarization, ohmic polarization, and cathode polarization, indicating that research attention should be paid to the cathode so that the cathode polarization can be substantially reduced. In brief, the spectacular cathode polarization can be attributed to the spontaneous establishment of an internal hydrogen peroxide-based fuel cells due to hydrogen peroxide self-decomposition. Therefore, to synthesize an appropriate and efficient electrocatalyst for the direct reduction of hydrogen peroxide is the future direction. In addition, the ohmic polarization is negligible in the low current density region but becomes notable in the high current density region.

### 3.3. Effect of EG concentration

Particularly, the species concentrations exhibit significant effects on the cell performance when the fuel cell design is determined. Figure 4 (a) displays the effect of EG concentration on the cell performance. When the EG concentration increases from 0.5 M to 2.0 M, the OCV increases with the EG concentration. It is because a higher EG concentration will result in the more EG adsorbed on the active sites on the catalyst due to the enhanced mass transport of EG, which is evidenced by the Figure 4 (c). Hence, the electrochemical kinetics of the EGOR is enhanced and the concentration loss is reduced because of the higher EG concentration, which is consistent with results from Figure 4 (b) that the anode potential under 2.0-M operation is much lower than that under 0.5-M operation under open-circuit condition. It can be seen that the cell with 0.5 M EG supply yields the poorest performance among three EG concentrations. It can be explained that the cell is at starve state under 0.5-M operation due to the relatively low EG concentration on the active sites, as shown in Figure 4 (c). Hence, the insufficient EG supply leads to the

largest anode polarization, which is evident in Figure 4 (b). At around the limiting current region, the EG concentration reaches nearly zero and the anode polarization exponentially increases, resulting in the rapid voltage degradation. When the EG concentration increases to 1.0 M, the cell performance experiences a remarkable promotion in both the OCV and limiting current density. It is attributed to more abundant EG adsorbed on active sites as well as the mitigatory anode polarization comparing to the 0.5-M operation. When the EG concentration further increases from 1.0 M to 2.0 M, the cell performance under 2.0-M operation is superior than that under 1.0-M operation at a low current density region (< 1000 A $m^{-2}$), while it is inferior at medium and high current density regions (> 1000 A $m^{-2}$). This observation can be explained as follows. At the low current density region, the anode polarization under 2.0-M operation is lower than that under 1.0-M operation and ohmic polarization shows negligible effect on the cell performance. As a result, the positive effect on the cell performance derived from low anode polarization is stronger than the negative effect derived from the high internal resistance, so that the overall performance under 2.0-M operation is better than that under 1.0-M operation at the low current density region. However, the ohmic polarization becomes notable at the high current density region due to the linear relation between the ohmic polarization and the current density. Hence, at the high current density region, the positive effect on the cell performance derived from low anode polarization is not able to compensate the remarkable negative effect derived from the ohmic polarization. As a result, the overall performance under 2.0 M operation is worse than that under 1.0 M operation at the high current density region.

### 3.4. Effect of NaOH concentration

It has been realized that the addition of alkali in the anolyte can elevate the cell performance significantly, indicating that the NaOH concentration is an important parameter. Hence, the

effect of NaOH concentration on the cell performance is studied and the results are presented in Figure 5 (a). It is found that the OCV increases with the NaOH concentration increasing from 1.0 M to 7.0 M as expected. It is attributed to the fast transport of $OH^-$ to the active sites with higher feeding concentration, so that the $OH^-$ concentration on the active sites is higher, as evidenced in Figure 5 (c). As a consequence, the anode polarization at open-circuit state is lower due to the faster EGOR kinetics as well as the limited concentration loss, as depicted in Figure 5 (b). After the cell is discharging, the cell under 1.0 M operation shows the worst performance. The reason for this phenomenon is the relatively low $OH^-$ concentration on the active sites, as shown in Figure 5 (c). Hence, the cell undergoes severe concentration loss, which causes the rapid voltage to decline in the range of 600 to 800 A $m^{-2}$. When further increasing the $OH^-$ concentration, the cell performances under 3.0-M, 5.0-M, and 7.0-M operation are similar at the current density range of 0 to 1600 A $m^{-2}$. The cell performance under 3.0-M operation exhibits an obvious degradation, which is attributed to the conspicuously increased anode overpotential, as presented in Figure 5 (b). Figure 5 (c) indicates that the $OH^-$ concentration reaches nearly zero at the current density higher than 2000 A $m^{-2}$, accounting for the notable anode overpotential due to the presence of the serious concentration loss. It is seen from Figure 5 (b) and Figure 5 (c) that the anode polarizations under 5.0-M and 7.0-M operation do not show huge difference, and the $OH^-$ concentrations on the active sites both are sufficient. However, the performance under 7.0-M operation is inferior comparing to that under 5.0-M operation at high current densities. This is because the ohmic loss will play a non-negligible role in the cell performance. As the internal resistance increases with the $OH^-$ concentration, the large ohmic loss results in the performance degradation.

### 3.5. Effect of $H_2O_2$ concentration

In this type of fuel cell, hydrogen peroxide is used as oxidant in the cathode to replace the oxygen or air. Hence, the $H_2O_2$ concentration is bound to an important parameter, which possesses critical effect on the cell performance. Figure 6 (a) exhibits the polarization curves with various $H_2O_2$ feeding concentration. It is found that the OCV increases when the $H_2O_2$ concentration is elevated from 1.0 M to 4.0 M, which can be ascribed to the lower cathode overpotential with higher $H_2O_2$ concentration, as evidenced in Figure 6 (b). It should be noted that higher $H_2O_2$ concentration results in the higher cathode potential (around 0.85 V), but the cathode potential is still far below the theoretical cathode potential (1.78 V). The significant performance loss is because of the spontaneous establishment of an internal hydrogen peroxide fuel cell in the cathode bringing about the tremendous mixed potential. The cell performance increases with the $H_2O_2$ concentration as well. This observation can be explained as follows. On one hand, the transport of $H_2O_2$ will be facilitated when the $H_2O_2$ concentration becomes higher, so that the $H_2O_2$ concentration is higher at the active sites. On the other hand, the electrochemical kinetics of HPRR will be enhanced when the $H_2O_2$ concentration becomes higher, which can be confirmed by Figure 6 (b). For instance, at 1500 A $m^{-2}$, the cathode potentials under 1.0-M, 2.0-M, and 4.0-M operations are 0.17 V, 0.35 V, and 0.56 V, respectively. The huge cathode overpotential under 1.0-M operation plays the dominant role in the rapid voltage decline.

**3.6. Effect of sulfuric acid concentration**

Since $H^+$ ion is a necessary reactant in the HPRR process, the $H^+$ concentration is certain to have effect on the cell performance. The effects of $H^+$ concentration on the cell performance and the cathode potential are shown in Figure 7 (a) and Figure 7 (b), respectively. It is seen from Figure 7 (a) that the OCV increases with the $H^+$ concentration increasing from 0.5 M to 2.0 M, which can be attributed to the lower cathode overpotential with higher $H^+$ concentration, as evidenced in

Figure 6 (b). After the cell is discharging, the cell performance is increasing with the $H^+$ concentration as well. This phenomenon can be explained as follows. On one hand, the delivery of $H^+$ ions to the cathode CL will be elevated when the $H^+$ concentration increases, resulting in that the $H^+$ concentration is higher on the active sites. On the other hand, the electrochemical kinetics of HPRR will be enhanced when the $H^+$ concentration is higher, which can be confirmed by Figure 6 (b). For instance, at 1000 A $m^{-2}$, the cathode potentials under 0.5-M, 1.0-M, and 2.0-M operation are 0.29 V, 0.48 V, and 0.69 V, respectively. The prominent cathode overpotential under 0.5-M operation is believed to play the dominant role in the rapid voltage degradation.

**3.7. Effect of exchange current density**

For a given cell structure and a fixed operating condition, the cell performance mainly depends on the electrocatalytic activity of the anode and cathode catalysts, respectively. Generally, the exchange current density reflects the electrocatalytic activity of the catalyst. The effects of the anode exchange current density on the cell performance and the anode potential are demonstrated in Figure 8 (a) and Figure 8 (b). It is indicated from the Figure 8 (a) that the OCV increases with the anode exchange current density increasing from 1 to 100 A $m^{-2}$. In addition, the cell with higher anode exchange current density yields the superior performance over the whole current density range as well. The promotion is mainly attributed to the dramatic anode overpotential reduction, as shown in Figure 8 (b). The similar observation can be obtained when the cathode exchange current density increases. The higher cathode exchange current density results in higher OCV and superior cell performance over the whole current density range, as shown in Figures 9 (a) and (b). The improvement is also attributed to the significant cathode overpotential reduction. As a consequence, it is extremely critical to develop novel catalyst with high electrocatalytic activity towards EGOR and HPRR processes.

### 3.8. Effect of diffusion layer thickness

As the anode DL provides the channels for the EG and NaOH delivery, the anode DL thickness will affect the EG and NaOH transport process, and thus the cell performance. Therefore, the cell performance with different anode DL thickness is studied, and the results are depicted in Figure 10 (a). The cell performance decreases along with the increased anode DL thickness from 500 to 2000 μm over the whole current density range. This trend can be ascribed to the fact that a thicker anode DL will increase the transfer length in the anode DL, thus the mass-transport resistance is enhanced simultaneously as expected. Therefore, for a given anolyte, less reactants are able to reach the active sites to participate in the EGOR process, resulting in the enlarged anode overpotential, as demonstrated in Figure 10 (b). In addition, it is also difficult for the products to remove from the cell, which is disadvantageous for achieving a satisfactory cell performance. Hence, the cell voltage experiences an obvious degradation when the anode DL thickness increases. As for the cathode DL thickness, the results from Figures 11 (a) and (b) show that the increase in the cathode DL thickness will increase the cathode overpotential, and thus decrease the cell voltage, which is similar to the anode DL thickness. It is worth mentioning that the DL also serves as a CL supporter. Too thin will result in the insufficient support for the CL, thus it is difficult to achieve the desired catalyst loading. In addition, the coated catalyst may suffer from severe loss with the cell operation due to the weak interaction between the catalyst particles and the DL. Hence, it is necessary to take all the parameters into consideration in practical application so that the diffusion layer thickness can be determined.

## 4. Concluding remarks

A one-dimensional mathematical model for the DEGFC with hydrogen peroxide as oxidant is developed. Various physicochemical processes are involved in this fuel cell, including

mass/charge transport and several electrochemical reactions. These processes are taken into consideration in the model, and the model results show a good agreement with the experimental data. The voltage loss is investigated first, and the results show that the cathode polarization exhibits the severest voltage loss, which can be attributed to the internal hydrogen peroxide-based fuel cell in cathode. Meanwhile, the effects of operating conditions and electrode structural parameters are investigated. The results show that the cell performance improves initially with the increasing concentration of EG and $OH^-$, while undergoing a decline at the high current density region, which might be attributed to the enhanced ohmic loss. In addition, the cell performance increases over the whole current density region with increasing hydrogen peroxide and $H^+$ concentrations. Meanwhile, the numerical results exhibit that the cell performance is elevated when the anode exchange current density or the cathode exchange current density is increasing from 1 to 100 A $m^{-2}$, which emphasizes the significance of developing novel catalyst with superior catalytic activity. Moreover, the effect of the structural parameter of anode and cathode DL on the cell performance is investigated, including the thickness of both anode and cathode DL. As shown by the numerical results, the increase of DL thickness in both anode and cathode has a negative effect on the cell performance. The resistance of mass-transport increases with when the DL becomes thicker, and influences both the delivery of reactants and the removal of reaction products. Future research attention will be mainly paid to developing more precise and advanced theory for the effect of the competitive adsorption on reaction kinetics.

**Acknowledgement:**

This work was fully supported by a grant from the Research Grants Council of the Hong Kong Special Administrative Region, China (Project No. 25211817).

**References**

[1] C. Lamy, A. Lima, V. LeRhun, F. Delime, C. Coutanceau, J.-M. Léger, Recent advances in the development of direct alcohol fuel cells (DAFC), Journal of Power Sources 105 (2002) 283-296.

[2] C. Bianchini, P.K. Shen, Palladium-based electrocatalysts for alcohol oxidation in half cells and in direct alcohol fuel cells, Chemical Reviews 109 (2009) 4183-4206.

[3] E. Antolini, E. Gonzalez, Alkaline direct alcohol fuel cells, Journal of Power Sources 195 (2010) 3431-3450.

[4] D. Sebastian, A. Serov, I. Matanovic, K. Artyushkova, P. Atanassov, A. Aricò, V. Baglio, Insights on the extraordinary tolerance to alcohols of Fe-NC cathode catalysts in highly performing direct alcohol fuel cells, Nano Energy 34 (2017) 195-204.

[5] L. An, T.S. Zhao, Anion exchange membrane fuel cells: Principles, Materials and Systems, Springer International Publishing, Cham, Switzerland, 2018.

[6] X. Chen, T. Li, J. Shen, Z. Hu, From structures, packaging to application: a system-level review for micro direct methanol fuel cell, Renewable and Sustainable Energy Reviews 80 (2017) 669-678.

[7] S.S. Munjewar, S.B. Thombre, R.K. Mallick, Approaches to overcome the barrier issues of passive direct methanol fuel cell–Review, Renewable and Sustainable Energy Reviews 67 (2017) 1087-1104.

[8] A. Chamaani, N. Chawla, M. Safa, B. El-Zahab, One-Dimensional Glass Micro-Fillers in Gel Polymer Electrolytes for Li-O-2 Battery Applications, Electrochimica Acta 235 (2017) 56-63.

[9] L. An, T. Zhao, Y. Li, Carbon-neutral sustainable energy technology: direct ethanol fuel cells, Renewable and Sustainable Energy Reviews 50 (2015) 1462-1468.

[10] Z.F. Pan, R. Chen, L. An, Y.S. Li, Alkaline anion exchange membrane fuel cells for cogeneration of electricity and valuable chemicals, Journal of Power Sources 365 (2017) 430-445.

[11] L. An, R. Chen, Recent progress in alkaline direct ethylene glycol fuel cells for sustainable energy production, Journal of Power Sources 329 (2016) 484-501.

[12] H. Yue, Y. Zhao, X. Ma, J. Gong, Ethylene glycol: properties, synthesis, and applications, Chemical Society Reviews 41 (2012) 4218-4244.

[13] A. Serov, C. Kwak, Recent achievements in direct ethylene glycol fuel cells (DEGFC), Applied Catalysis B: Environmental 97 (2010) 1-12.

[14] C. Cremers, A. Niedergesäß, F. Jung, D. Müller, J. Tübke, Development of an alkaline anion exchange membrane direct ethylene glycol fuel cell stack, ECS Transactions 41 (2011) 1987-1996.

[15] L. Xin, Z. Zhang, J. Qi, D. Chadderdon, W. Li, Electrocatalytic oxidation of ethylene glycol (EG) on supported Pt and Au catalysts in alkaline media: Reaction pathway investigation in three-electrode cell and fuel cell reactors, Applied Catalysis B: Environmental 125 (2012) 85-94.

[16] O.O. Fashedemi, H.A. Miller, A. Marchionni, F. Vizza, K.I. Ozoemena, Electro-oxidation of ethylene glycol and glycerol at palladium-decorated FeCo@ Fe core–shell nanocatalysts for alkaline direct alcohol fuel cells: functionalized MWCNT supports and impact on product selectivity, Journal of Materials Chemistry A 3 (2015) 7145-7156.

[17] L. An, T. Zhao, Z. Chai, L. Zeng, P. Tan, Modeling of the mixed potential in hydrogen peroxide-based fuel cells, International Journal of Hydrogen Energy 39 (2014) 7407-7416.

[18] L. An, C. Jung, Transport phenomena in direct borohydride fuel cells, Applied Energy 205 (2017) 1270-1282.

[19] Z.F. Pan, B. Huang, L. An, Performance of a hybrid direct ethylene glycol fuel cell, International Journal of Energy Research (2018).

[20] S. Fukuzumi, Y. Yamada, Hydrogen Peroxide used as a Solar Fuel in One-Compartment Fuel Cells, ChemElectroChem 3 (2016) 1978-1989.

[21] X. Yan, P. Gao, G. Zhao, L. Shi, J. Xu, T. Zhao, Transport of highly concentrated fuel in direct methanol fuel cells, Applied Thermal Engineering 126 (2017) 290-295.

[22] B. Wang, Y. Zhou, Q. Du, Y. Yin, K. Jiao, Transient investigation of passive alkaline membrane direct methanol fuel cell, Applied Thermal Engineering 100 (2016) 1245-1258.

[23] Y. Yu, X. Yang, Y. Zhao, X. Zhang, L. An, M. Huang, G. Chen, R. Zhang, Engineering the Band Gap States of the Rutile TiO2 (110) Surface by Modulating the Active Heteroatom, Angewandte Chemie (2018).

[24] G. Zhang, K. Jiao, Multi-phase models for water and thermal management of proton exchange membrane fuel cell: A review, Journal of Power Sources 391 (2018) 120-133.

[25] K. Jiao, X. Li, Water transport in polymer electrolyte membrane fuel cells, Progress in Energy and Combustion Science 37 (2011) 221-291.

[26] H. Bahrami, A. Faghri, Multi-layer membrane model for mass transport in a direct ethanol fuel cell using an alkaline anion exchange membrane, Journal of Power Sources 218 (2012) 286-296.

[27] T. Guo, J. Sun, J. Zhang, H. Deng, X. Xie, K. Jiao, X. Huang, Transient analysis of passive vapor-feed DMFC fed with neat methanol, International Journal of Hydrogen Energy 42 (2017) 3222-3239.

[28] X. Xie, H. Yu, H. Deng, G. Zhang, T. Guo, J. Sun, K. Jiao, Modeling of passive vapor feed alkaline membrane direct methanol fuel cell, Applied Thermal Engineering 131 (2018) 920-932.

[29] B. Wang, K. Wu, Z. Yang, K. Jiao, A quasi-2D transient model of proton exchange membrane fuel cell with anode recirculation, Energy Conversion and Management 171 (2018) 1463-1475.

[30] S. Huo, J. Zhou, T. Wang, R. Chen, K. Jiao, Experimental and analytical analysis of polarization and water transport behaviors of hydrogen alkaline membrane fuel cell, Journal of Power Sources 382 (2018) 1-12.

[31] M.Z. Yu, S. Zhou, Y. Liu, Z.Y. Wang, T. Zhou, J.J. Zhao, Z.B. Zhao, J.S. Qiu, Long life rechargeable Li-O-2 batteries enabled by enhanced charge transfer in nanocable-like Fe@N-doped carbon nanotube catalyst, Science China-Materials 60 (2017) 415-426.

[32] L. An, T. Zhao, R. Chen, Q. Wu, A novel direct ethanol fuel cell with high power density, Journal of Power Sources 196 (2011) 6219-6222.

[33] R. Pathak, S. Basu, Mathematical modeling and experimental verification of direct glucose anion exchange membrane fuel cell, Electrochimica Acta 113 (2013) 42-53.

[34] R. Chen, T. Zhao, Mathematical modeling of a passive-feed DMFC with heat transfer effect, Journal of Power Sources 152 (2005) 122-130.

[35] J.P. Hoare, Oxygen Overvoltage Measurements on Bright Platinum in Acid Solutions II Bright Platinum in Stabilized Acid Solutions, Journal of The Electrochemical Society 112 (1965) 608-611.

[36] I. Katsounaros, W.B. Schneider, J.C. Meier, U. Benedikt, P.U. Biedermann, A.A. Auer, K.J. Mayrhofer, Hydrogen peroxide electrochemistry on platinum: towards understanding the oxygen reduction reaction mechanism, Physical Chemistry Chemical Physics 14 (2012) 7384-7391.

[37] S. Huo, J. Zhou, T. Wang, R. Chen, K. Jiao, Experimental and analytical analysis of polarization and water transport behaviors of hydrogen alkaline membrane fuel cell, Journal of Power Sources 382 (2018) 1-12.

[38] N. Bussayajarn, D.A. Harrington, S. Therdthianwong, A. Therdthianwong, N. Djilali, The cathodic polarization prediction of H 2/H 2 O 2 fuel cells by using EIS spectra, Paper A 12 (2004).

[39] S.B. Hall, E.A. Khudaish, A.L. Hart, Electrochemical oxidation of hydrogen peroxide at platinum electrodes. Part 1. An adsorption-controlled mechanism, Electrochimica Acta 43 (1998) 579-588.

[40] L. An, Z. Chai, L. Zeng, P. Tan, T. Zhao, Mathematical modeling of alkaline direct ethanol fuel cells, International Journal of Hydrogen Energy 38 (2013) 14067-14075.

[41] C. Xu, T. Zhao, Q. Ye, Effect of anode backing layer on the cell performance of a direct methanol fuel cell, Electrochimica Acta 51 (2006) 5524-5531.

[42] G. Ternström, A. Sjöstrand, G. Aly, Å. Jernqvist, Mutual diffusion coefficients of water+ ethylene glycol and water+ glycerol mixtures, Journal of Chemical & Engineering Data 41 (1996) 876-879.

[43] G.H. Miley, E.D. Byrd, in: Excerpt from the proceedings of the COMSOL users conference, 2006.

[44] J. Newman, K.E. Thomas-Alyea, Electrochemical systems, John Wiley & Sons, 2012.

[45] W. Yang, T. Zhao, A two-dimensional, two-phase mass transport model for liquid-feed DMFCs, Electrochimica Acta 52 (2007) 6125-6140.

[46] Z.F. Pan, L. An, T.S. Zhao, Z.K. Tang, Advances and challenges in alkaline anion exchange membrane fuel cells, Progress in Energy and Combustion Science 66 (2018) 141-175.

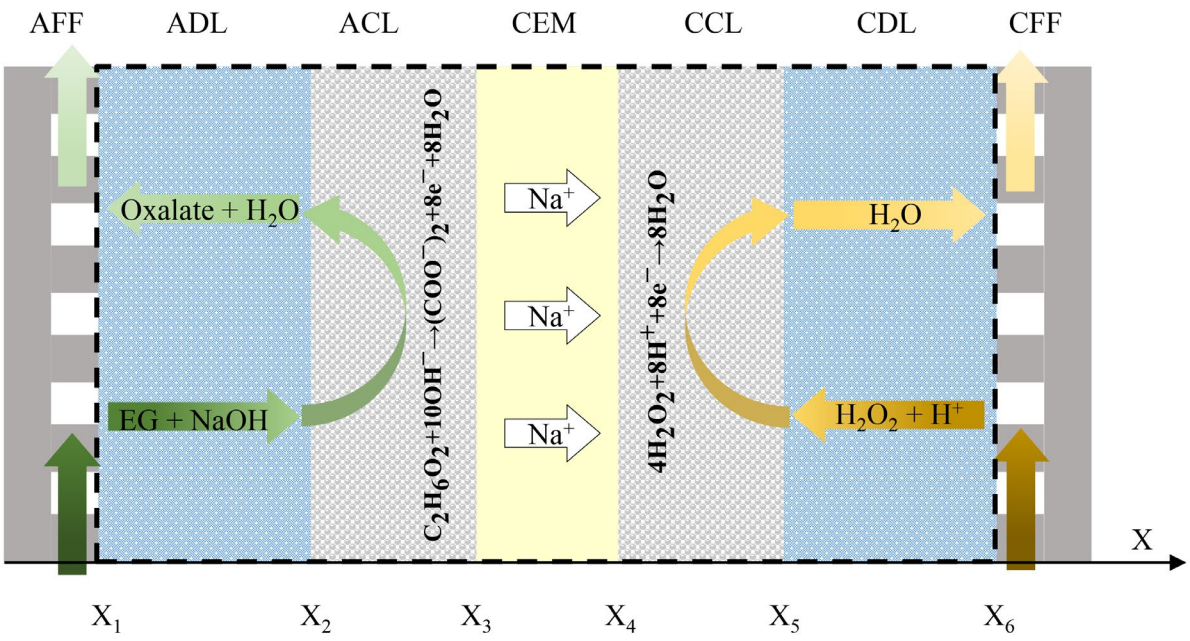


Figure 1 Schematic of a DEGFC and the coordinate system.

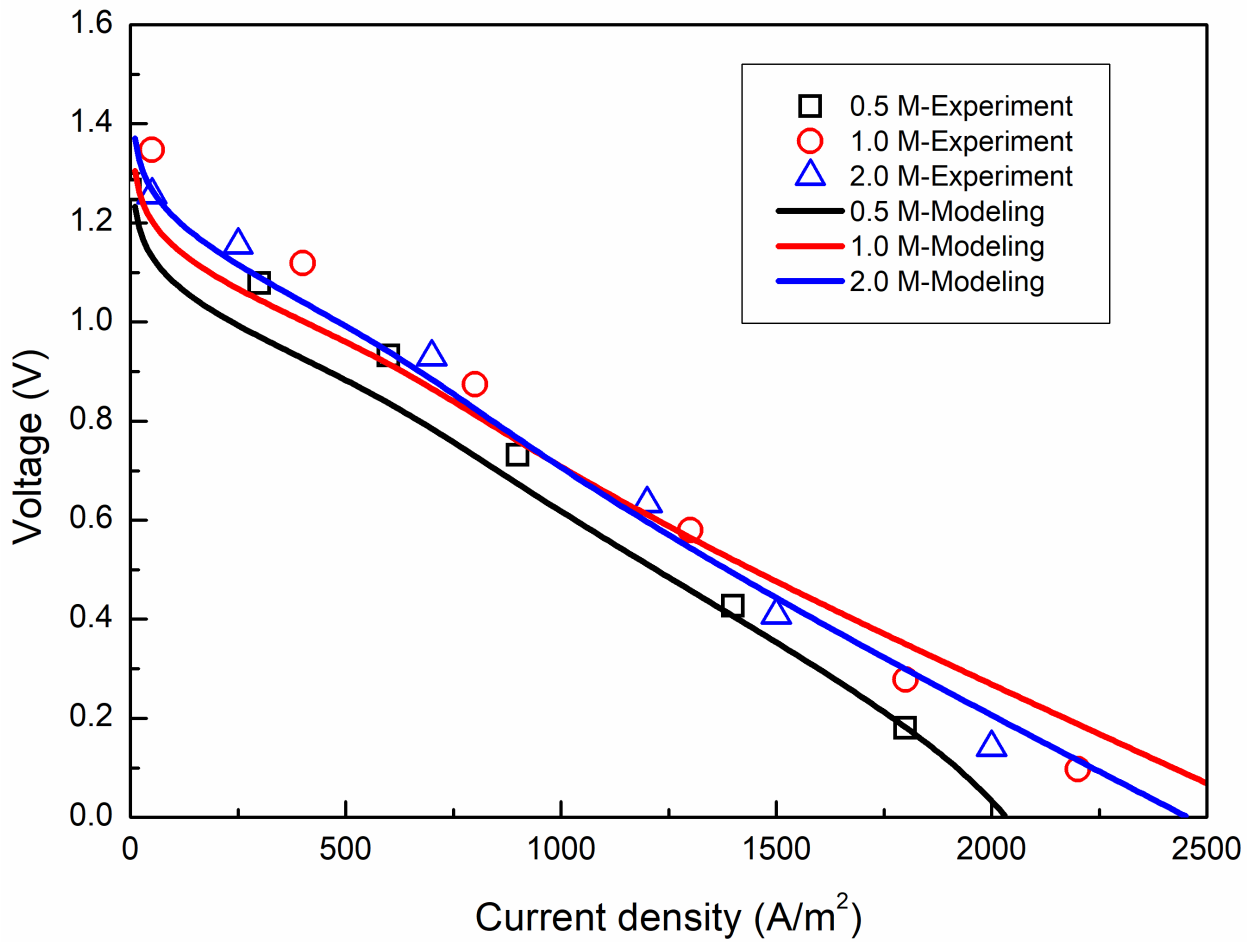


Figure 2 Validation made between numerical results and experimental data.

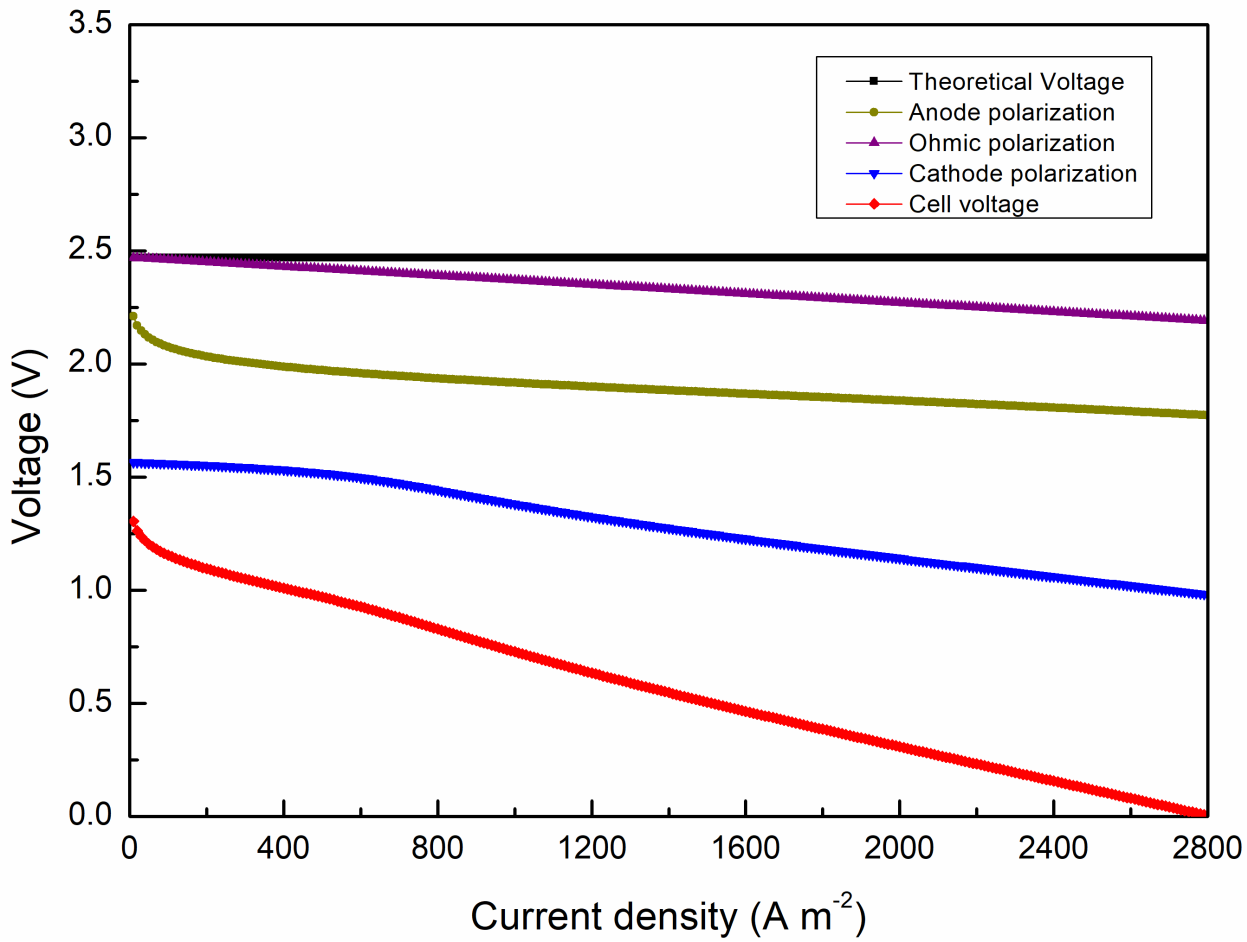


Figure 3 Specific polarizations and overall voltage loss with the current density.

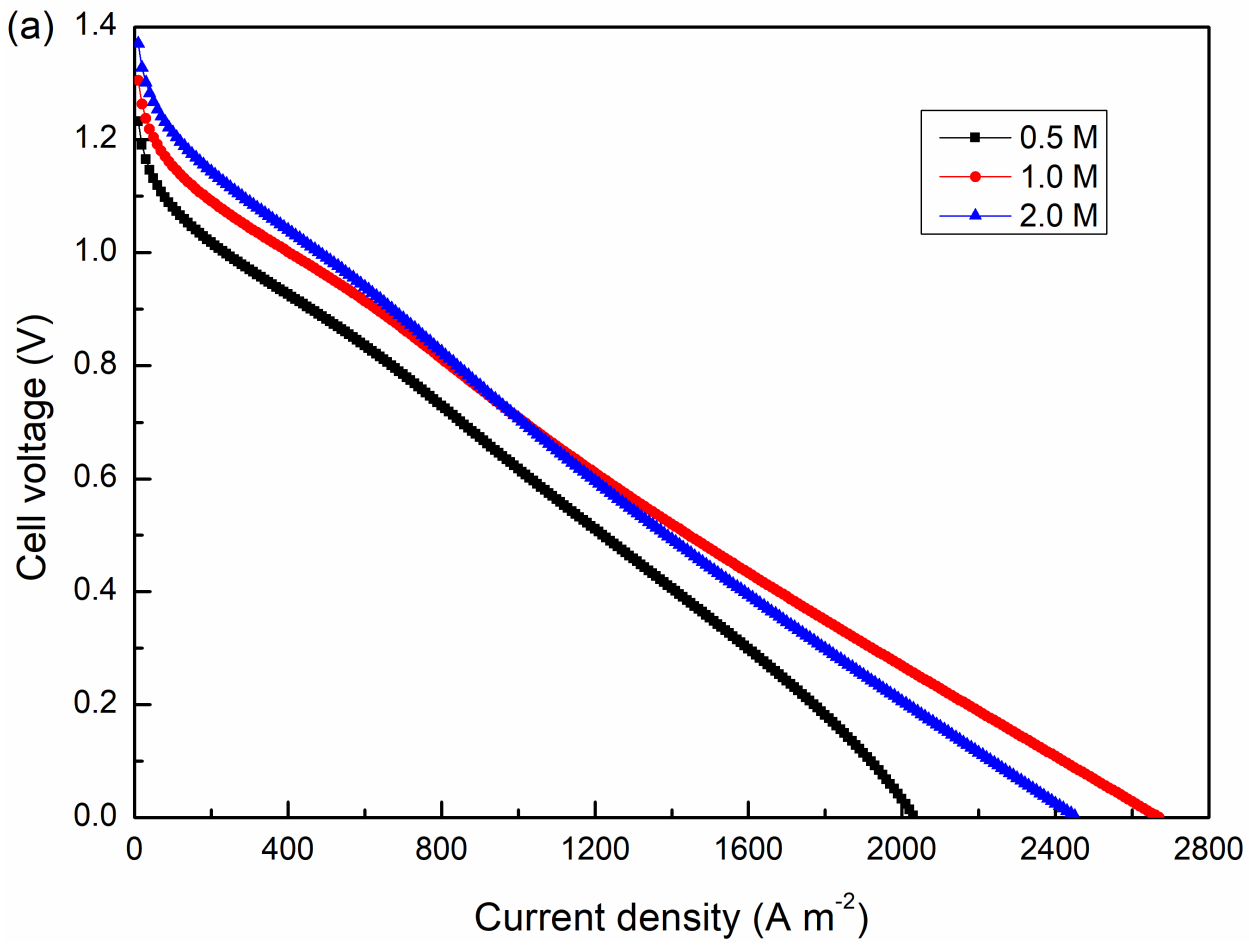
(a)
1.4
1.2
1.0
0.8
0.6
0.4
0.2
0.0
Cell voltage (V)
0
400
800
1200
1600
2000
2400
2800
Current density (A m-2)
0.5 M
1.0 M
2.0 M

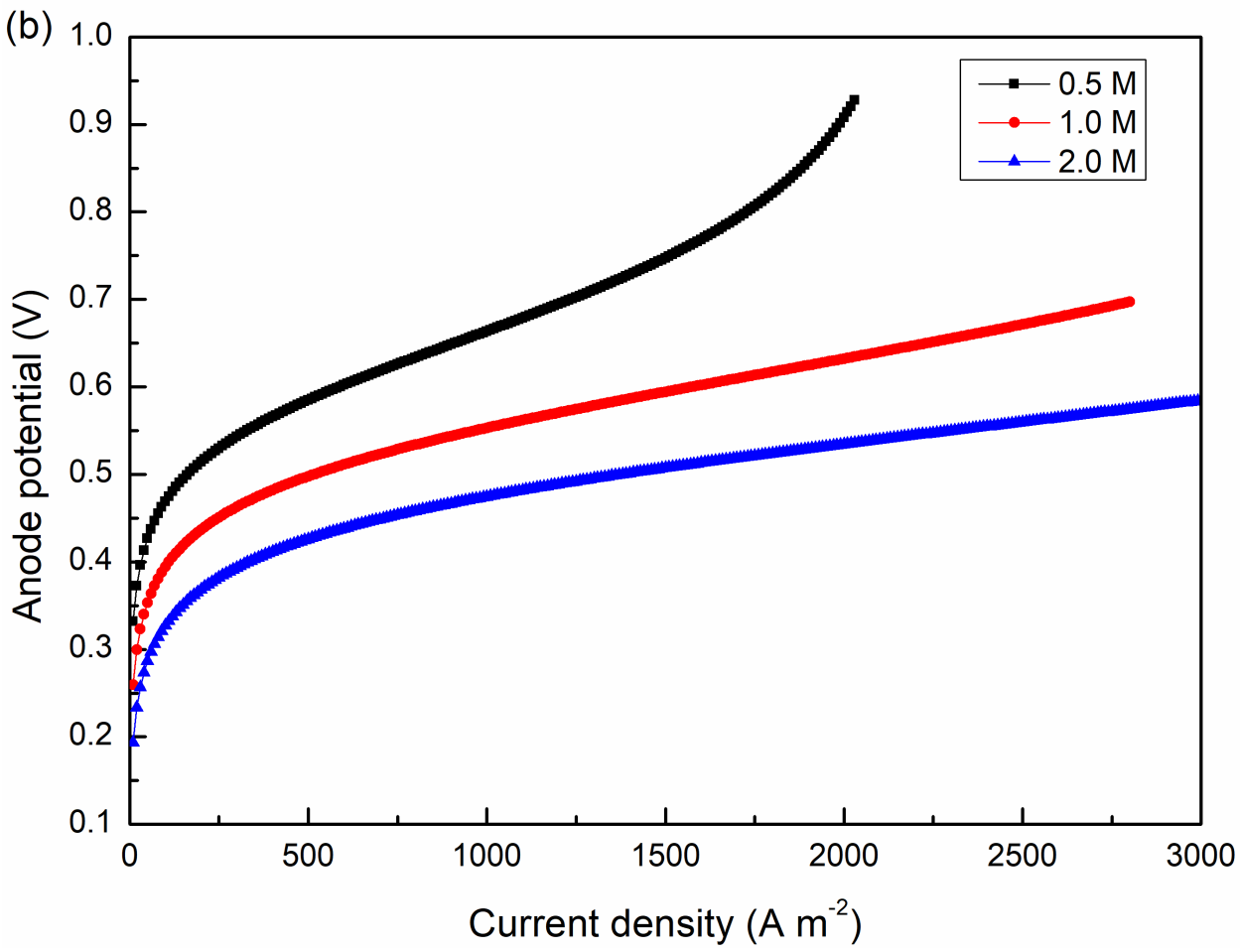
(b)
Anode potential (V)
Current density (A m-2)
0.5 M
1.0 M
2.0 M
1.0
0.9
0.8
0.7
0.6
0.5
0.4
0.3
0.2
0.1
0
500
1000
1500
2000
2500
3000

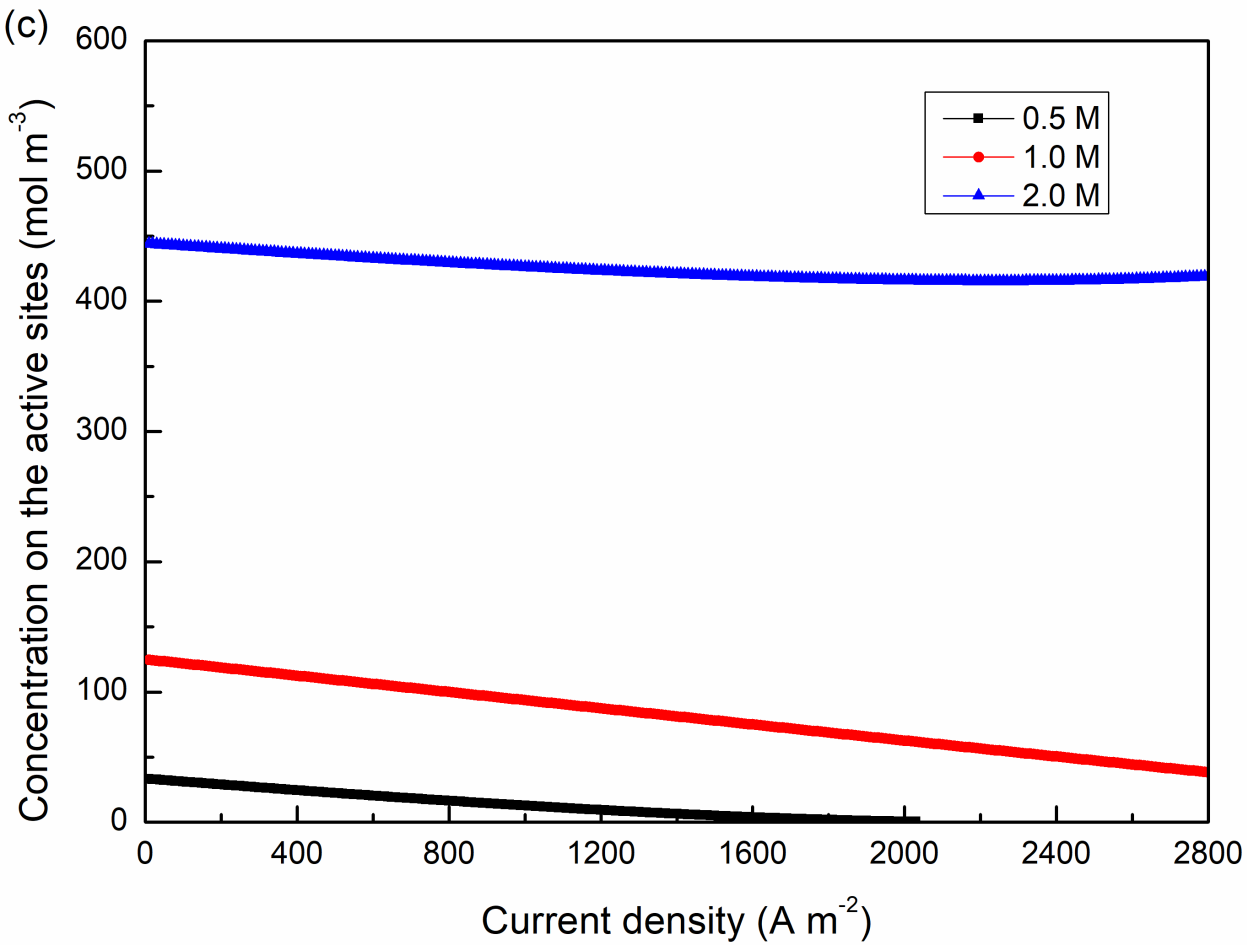


Figure 4 Effect of the EG concentration on the cell performance. (a) Polarization curves; (b) Anode overpotentials; and (c) Concentration on the active sites.

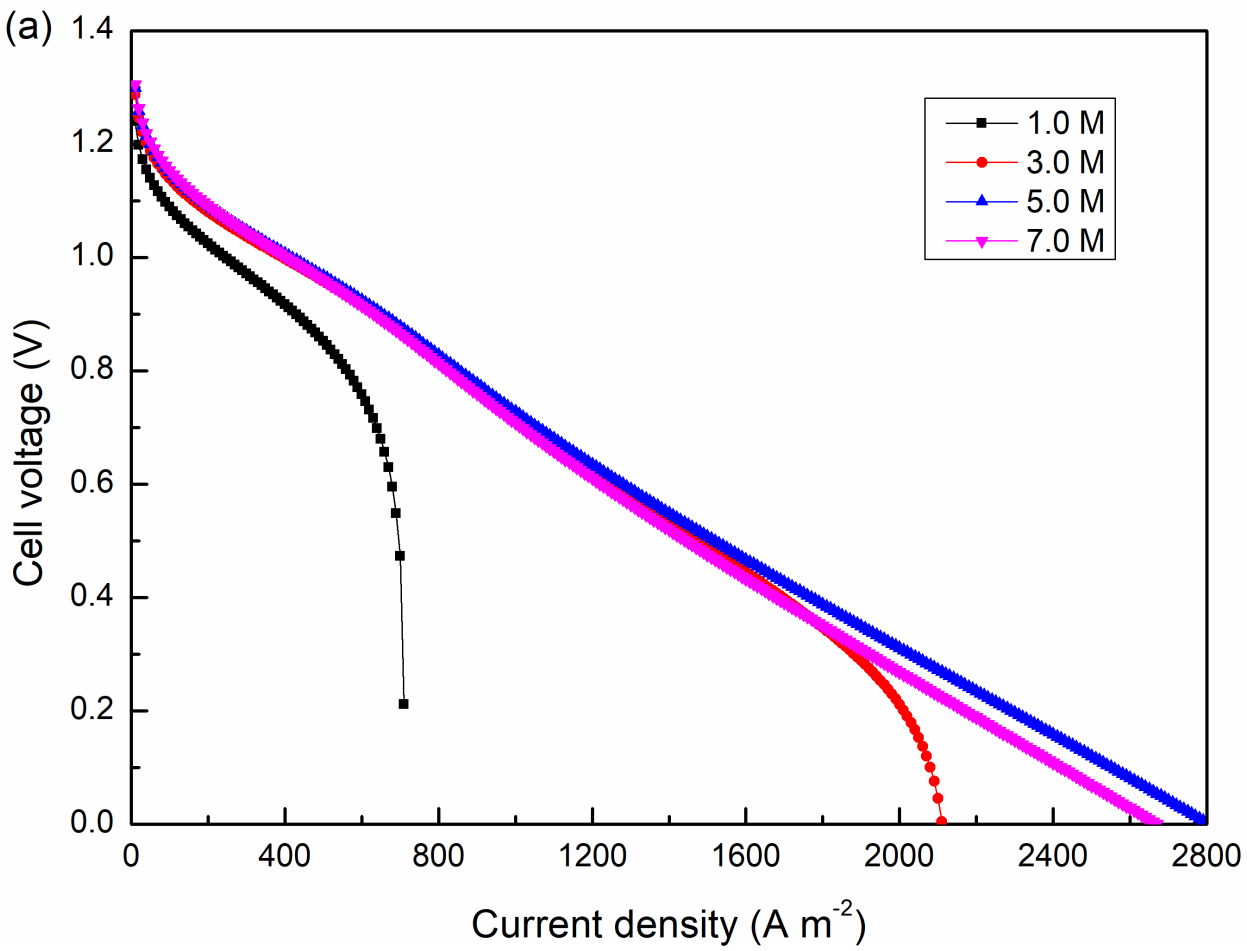
(a)
1.4
1.2
1.0
0.8
0.6
0.4
0.2
0.0
Cell voltage (V)
0
400
800
1200
1600
2000
2400
2800
Current density (A m-2)
1.0 M
3.0 M
5.0 M
7.0 M

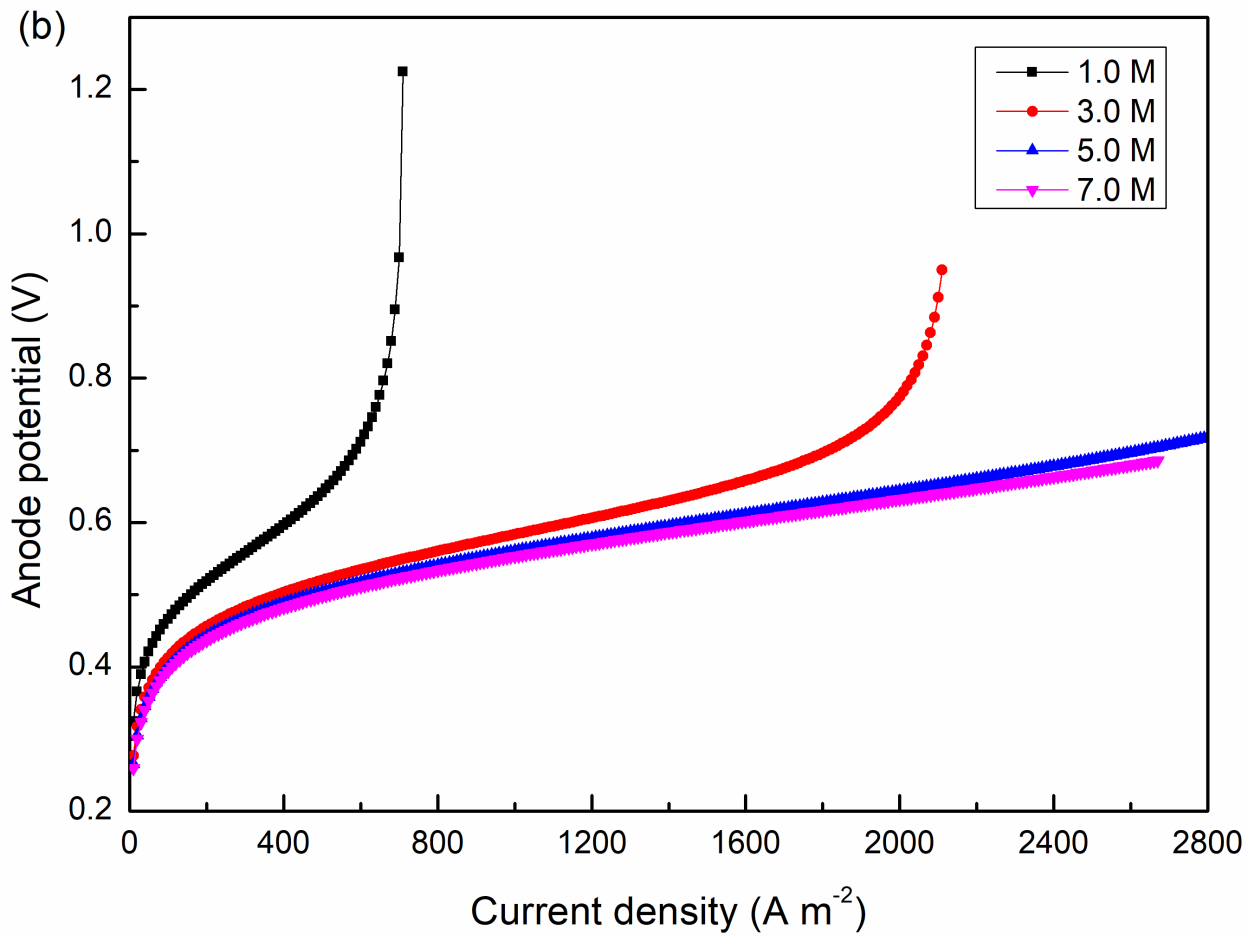
(b)
1.0 M
3.0 M
5.0 M
7.0 M
Anode potential (V)
1.2
1.0
0.8
0.6
0.4
0.2
0
400
800
1200
1600
2000
2400
2800
Current density (A m-2)

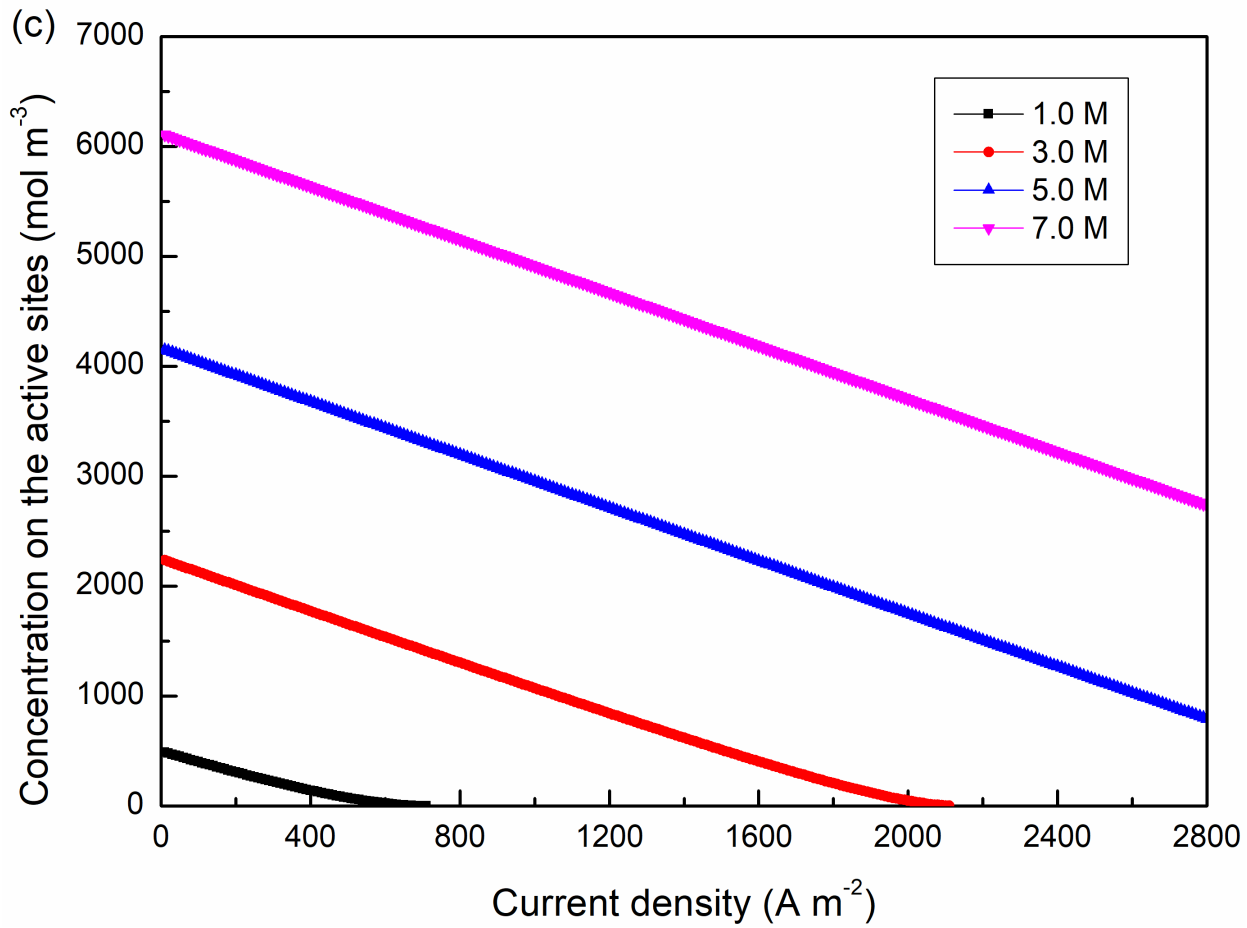


Figure 5 Effect of the hydroxyl ion concentration on the cell performance. (a) Polarization curves; (b) Anode overpotentials; and (c) Concentration on the active sites.

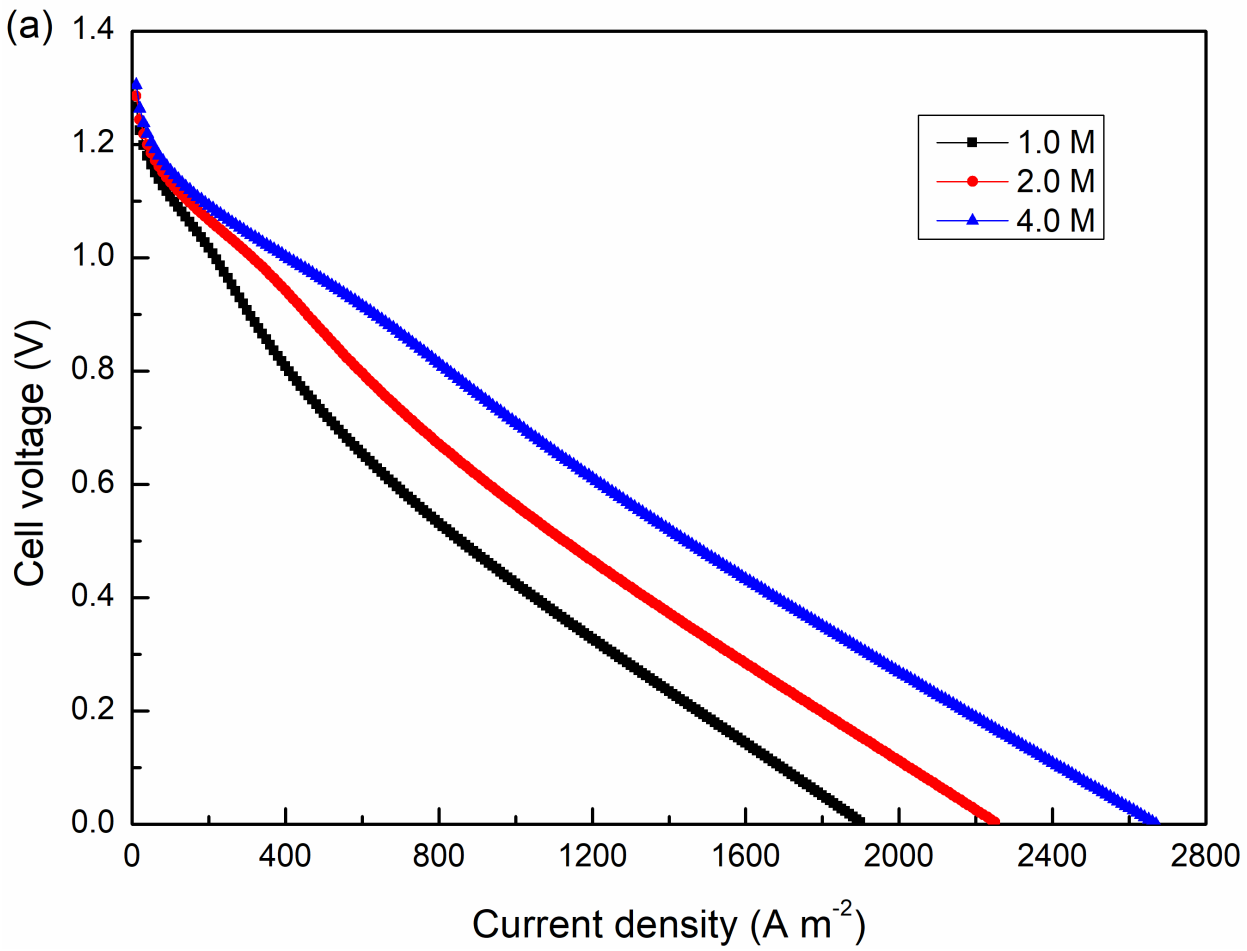
(a)
1.4
1.2
1.0
0.8
0.6
0.4
0.2
0.0
Cell voltage (V)
0
400
800
1200
1600
2000
2400
2800
Current density (A m-2)
1.0 M
2.0 M
4.0 M

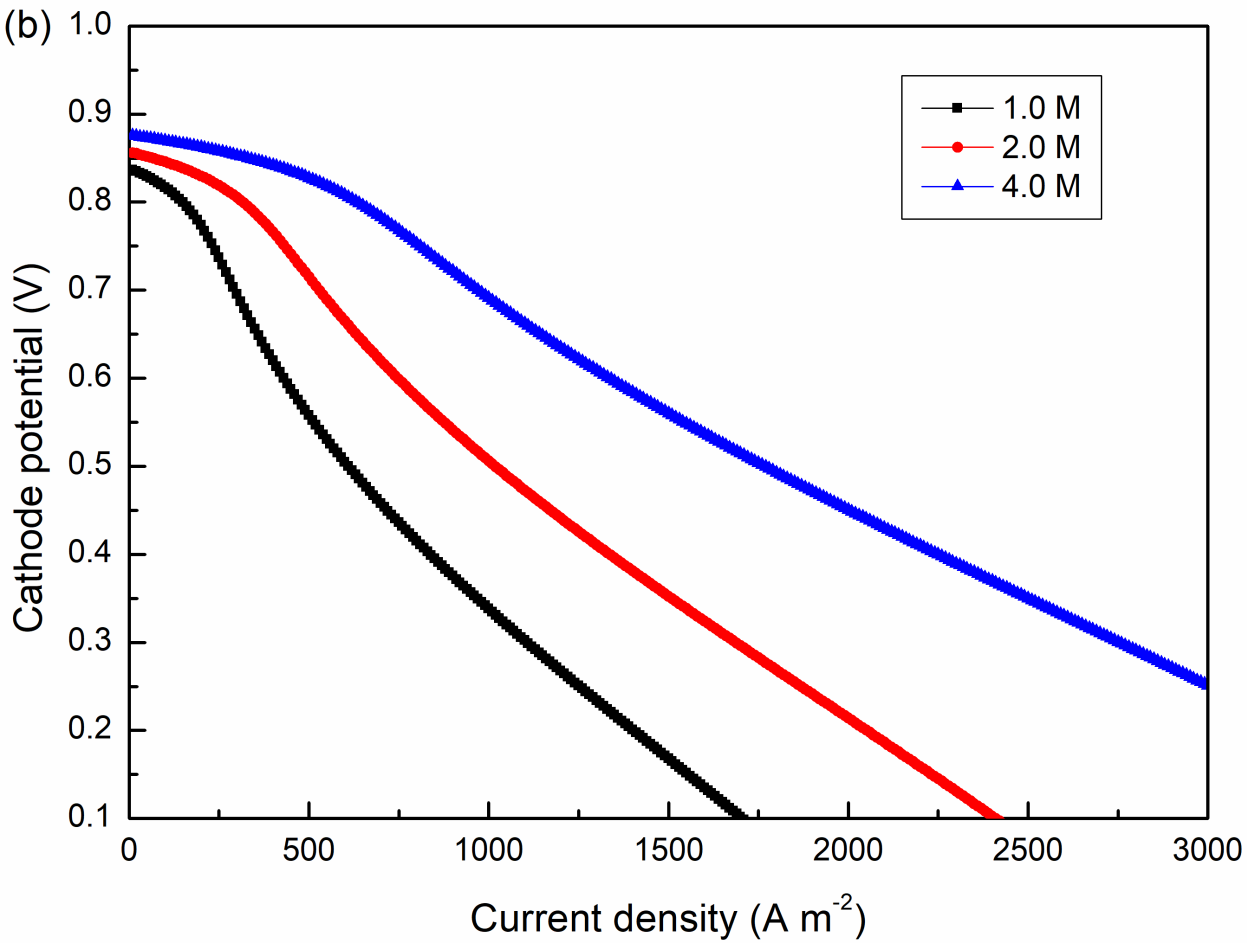


Figure 6 Effect of the hydrogen peroxide concentration on the cell performance. (a) Polarization curves; and (b) Cathode overpotentials.

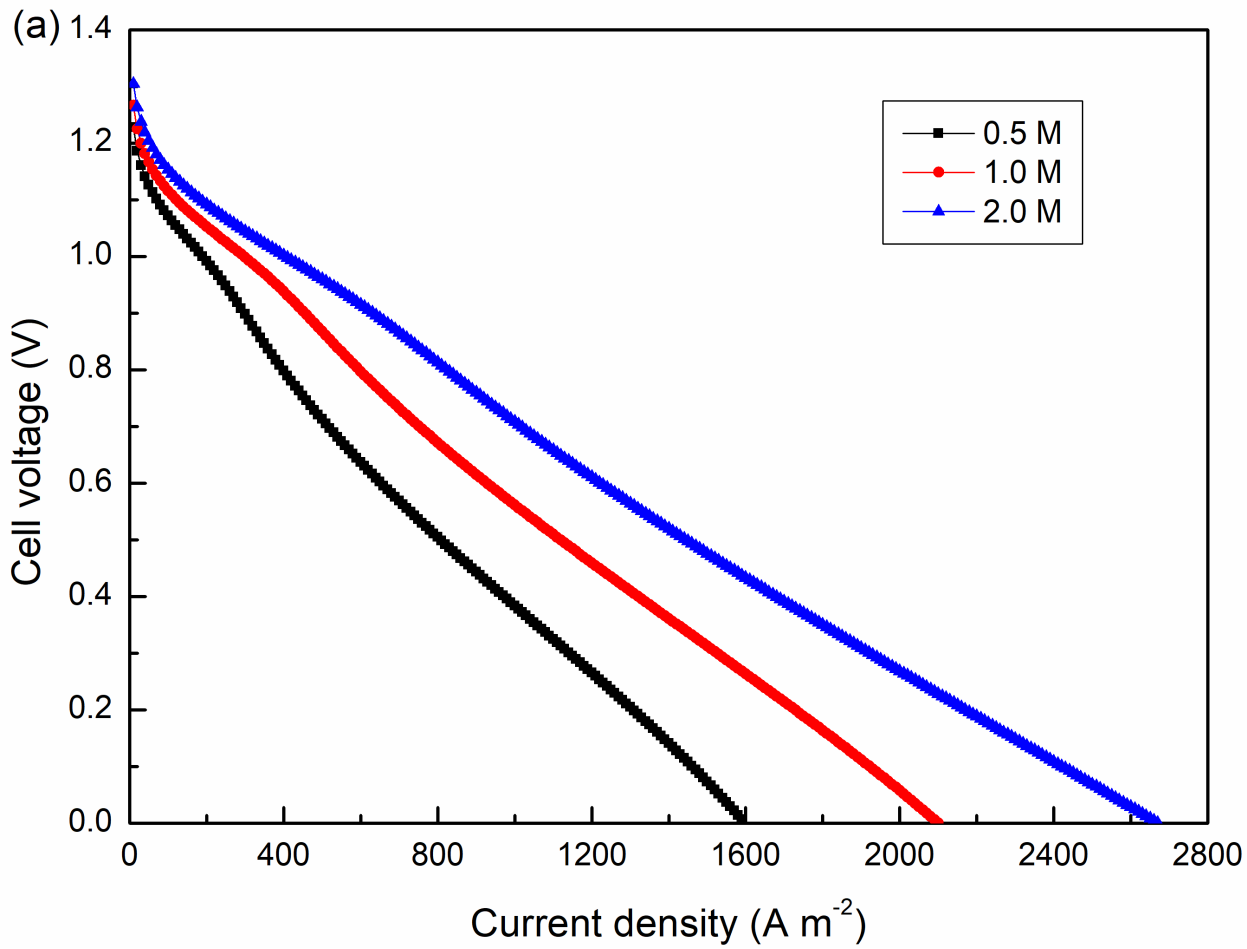
(a)
1.4
1.2
1.0
0.8
0.6
0.4
0.2
0.0
Cell voltage (V)
0
400
800
1200
1600
2000
2400
2800
Current density (A m-2)
0.5 M
1.0 M
2.0 M

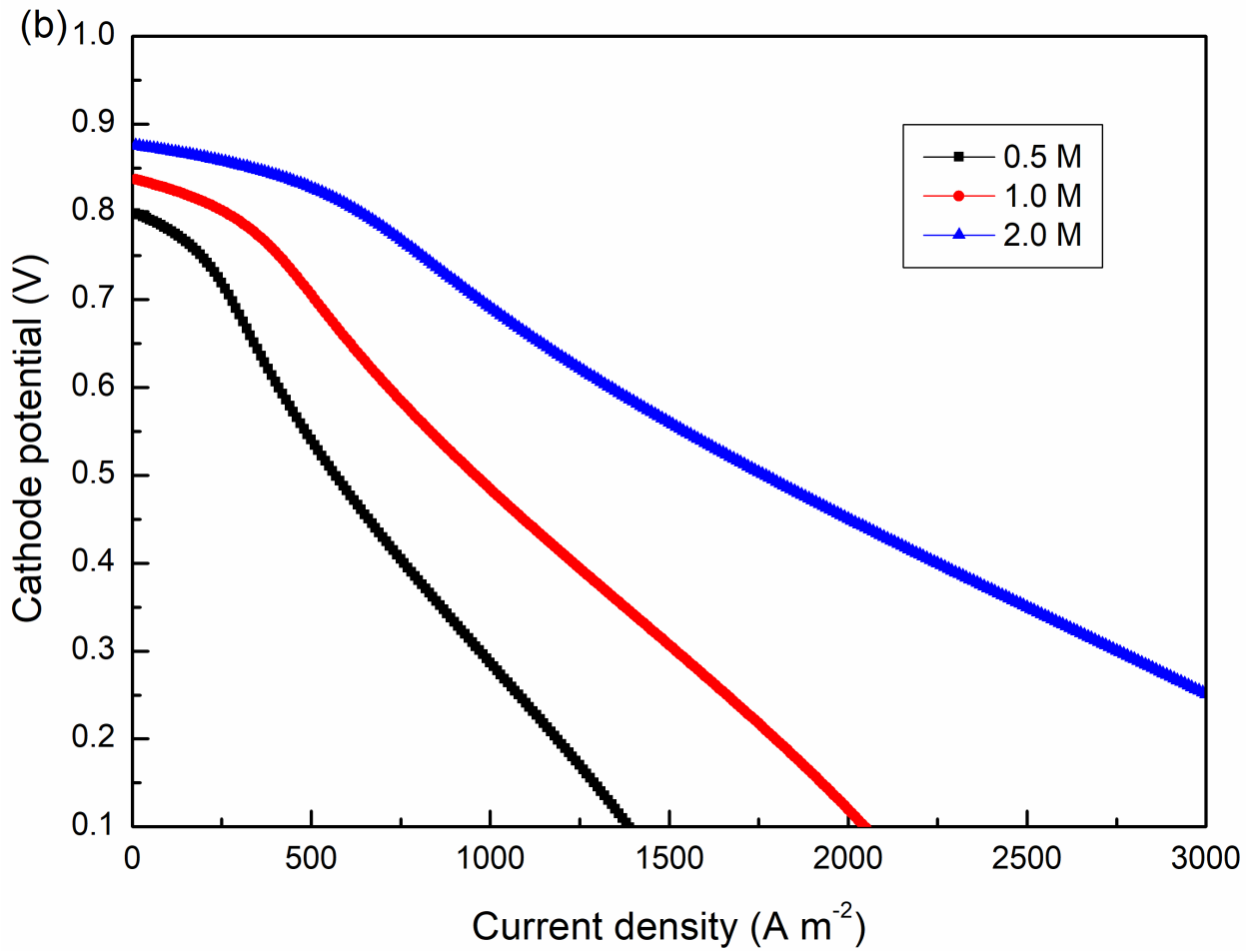


Figure 7 Effect of the $H^+$ concentration on the cell performance. (a) Polarization curves; and (b) Cathode overpotentials.

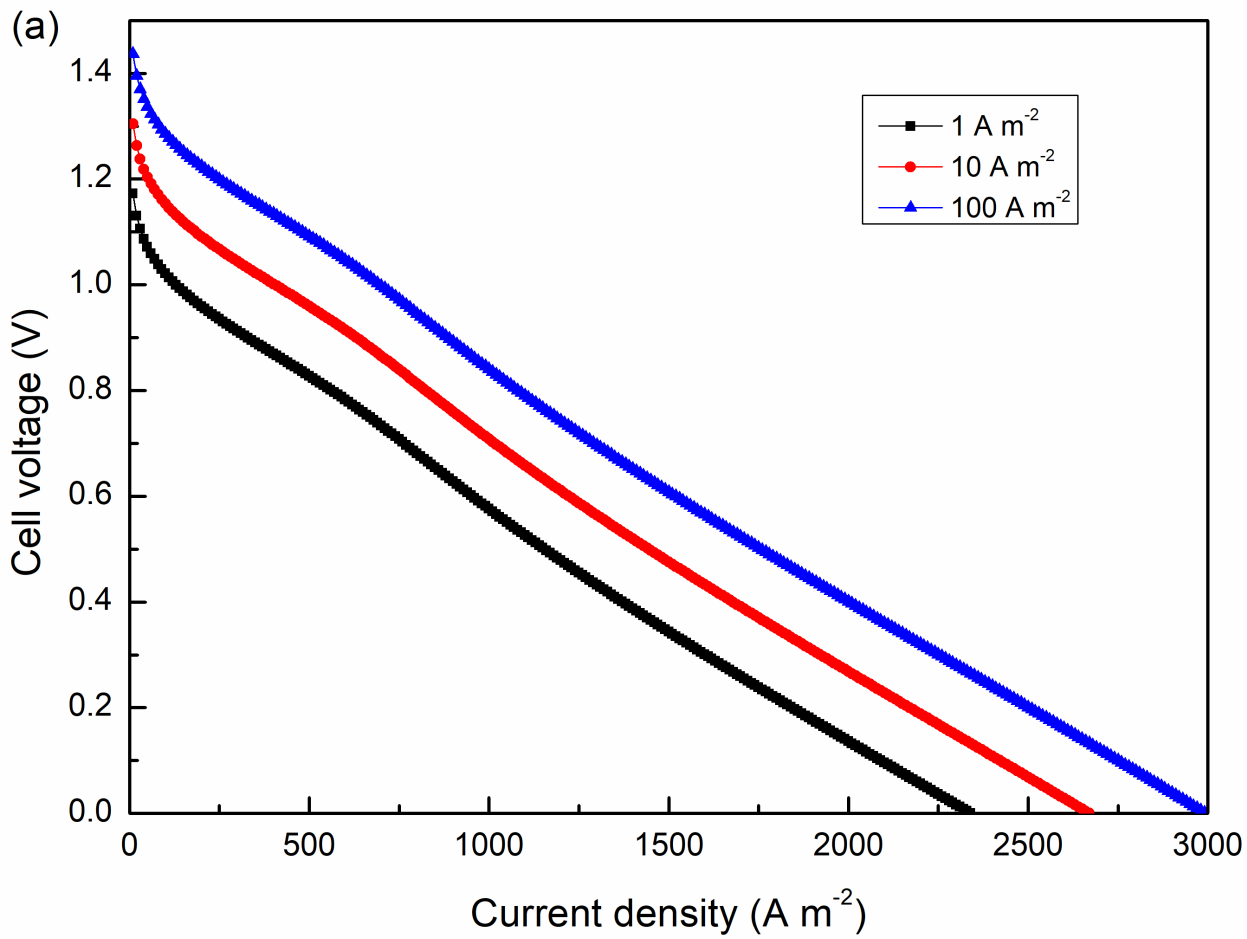
(a)
Cell voltage (V)
Current density (A m-2)
1 A m-2
10 A m-2
100 A m-2
0.0
0.2
0.4
0.6
0.8
1.0
1.2
1.4
0
500
1000
1500
2000
2500
3000

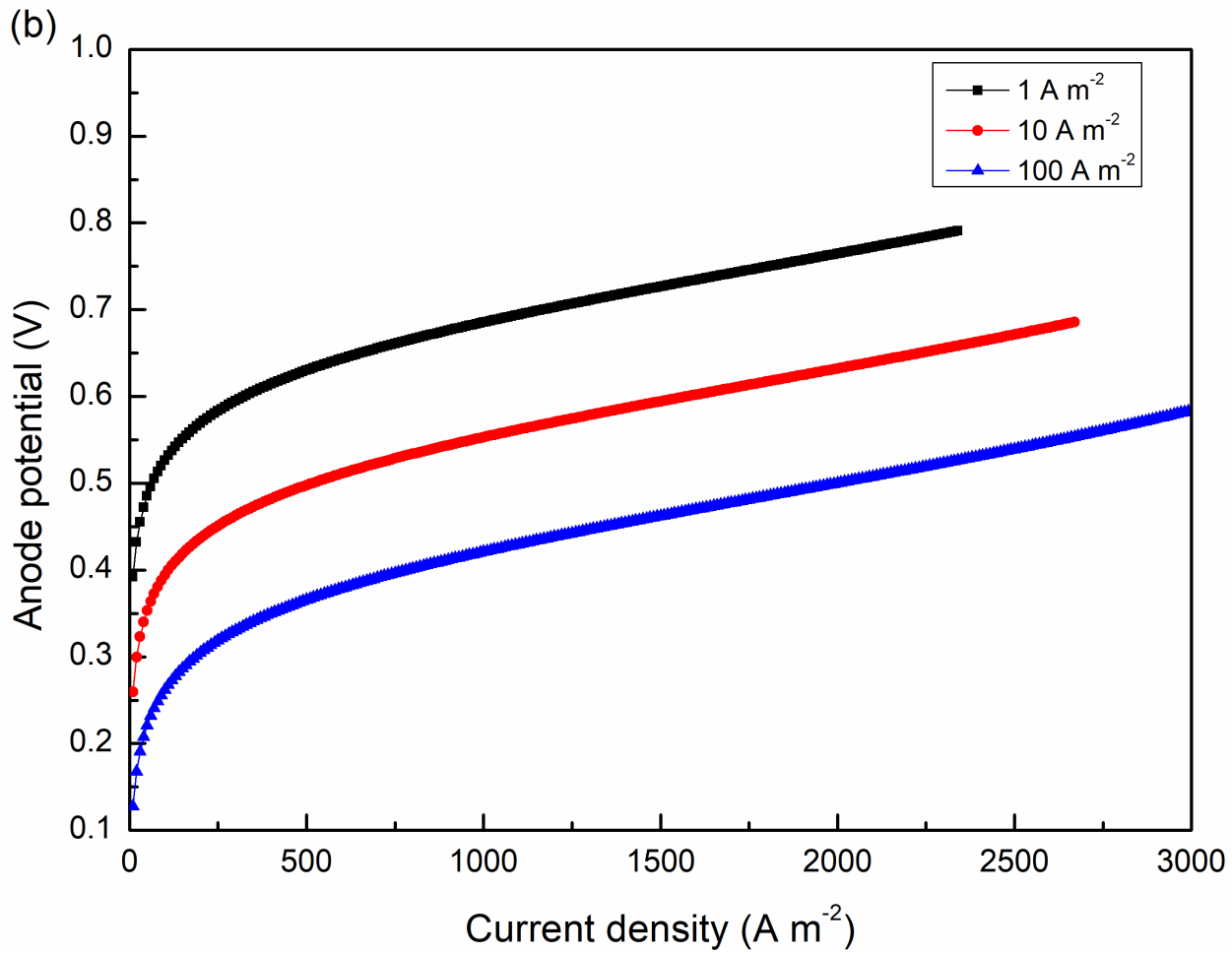


Figure 8 Effect of the anode exchange current density on the cell performance. (a) Polarization curves; and (b) Anode overpotentials.

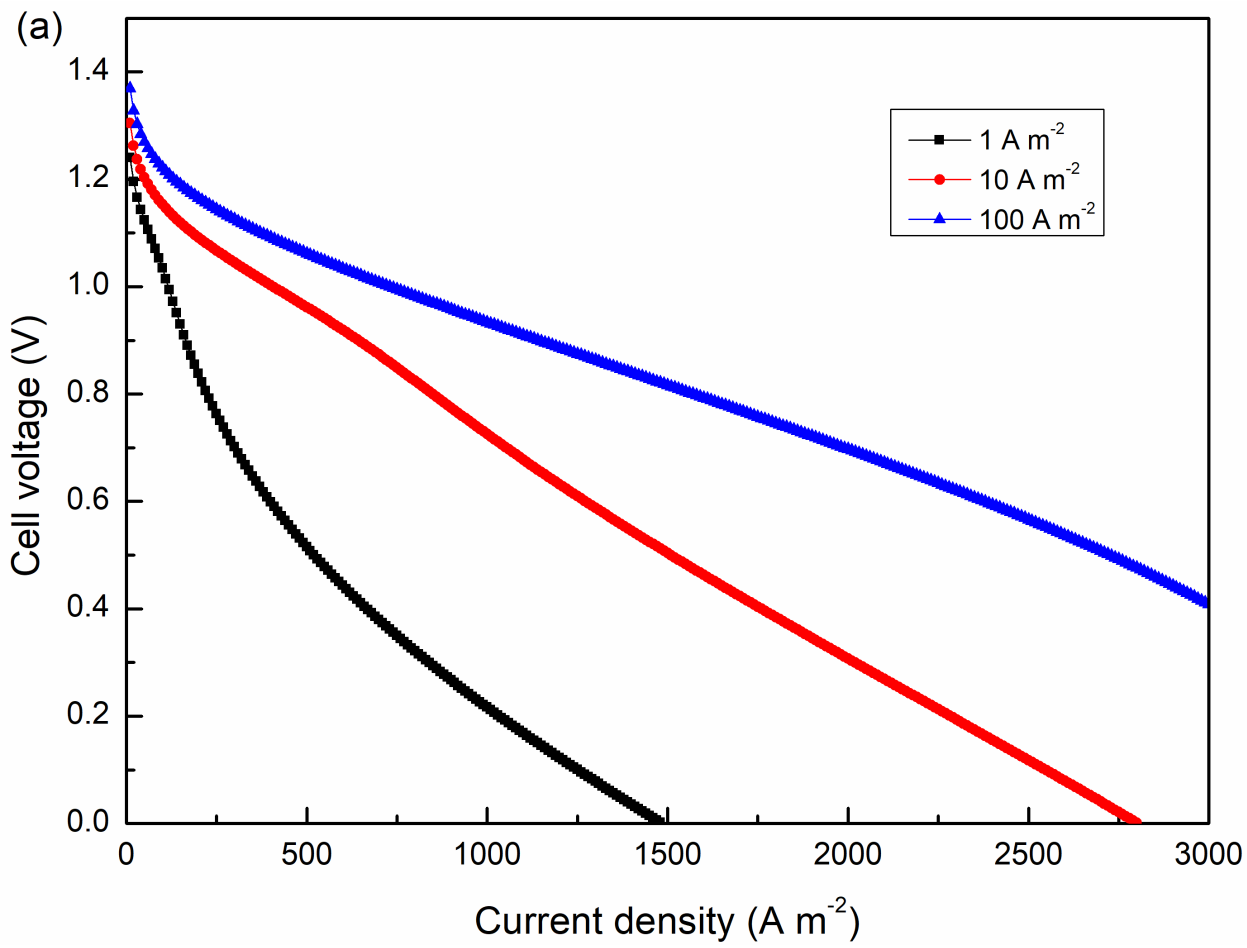
(a)
1.4
1.2
1.0
0.8
0.6
0.4
0.2
0.0
Cell voltage (V)
0
500
1000
1500
2000
2500
3000
Current density (A m-2)
1 A m-2
10 A m-2
100 A m-2

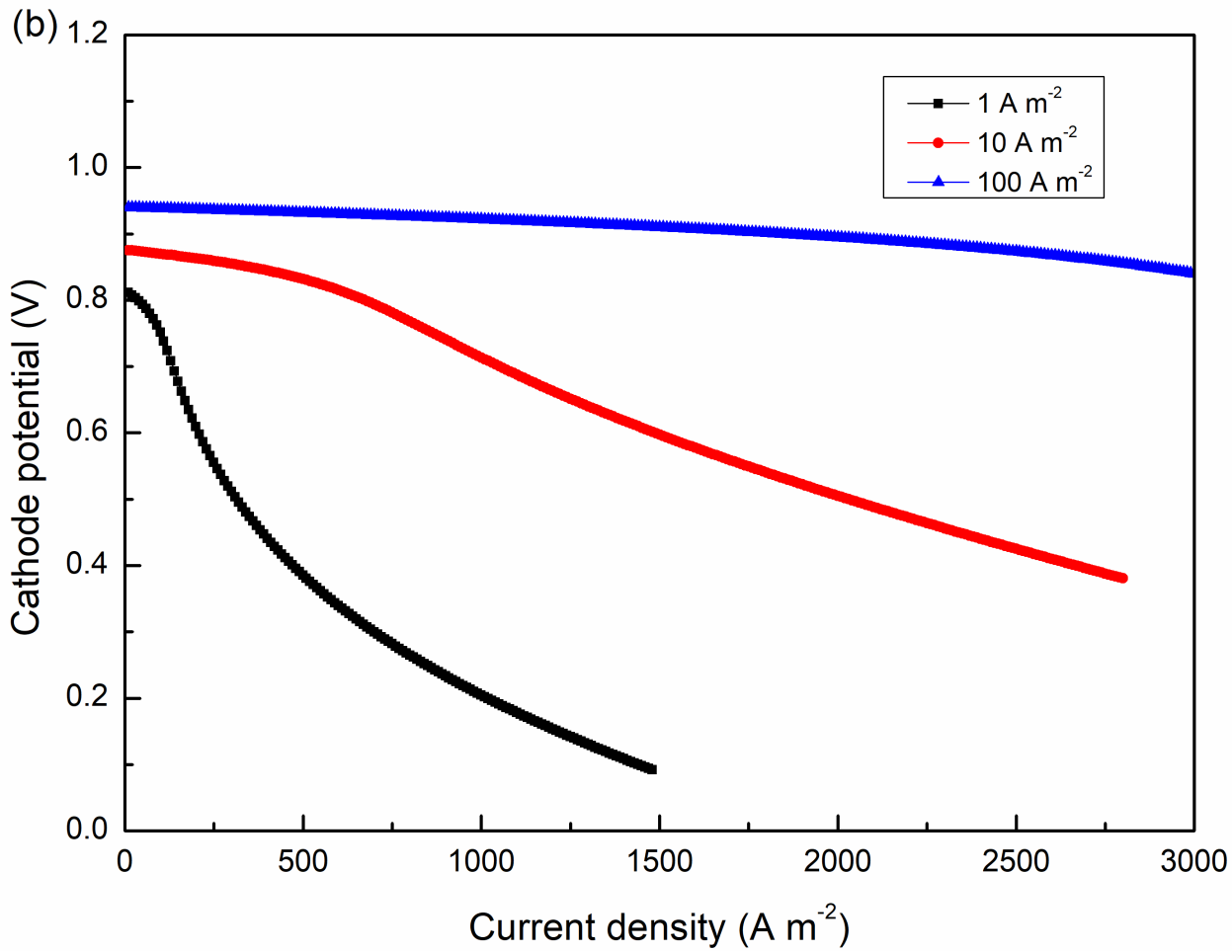


Figure 9 Effect of the cathode exchange current density on the cell performance. (a) Polarization curves; and (b) Cathode overpotentials.

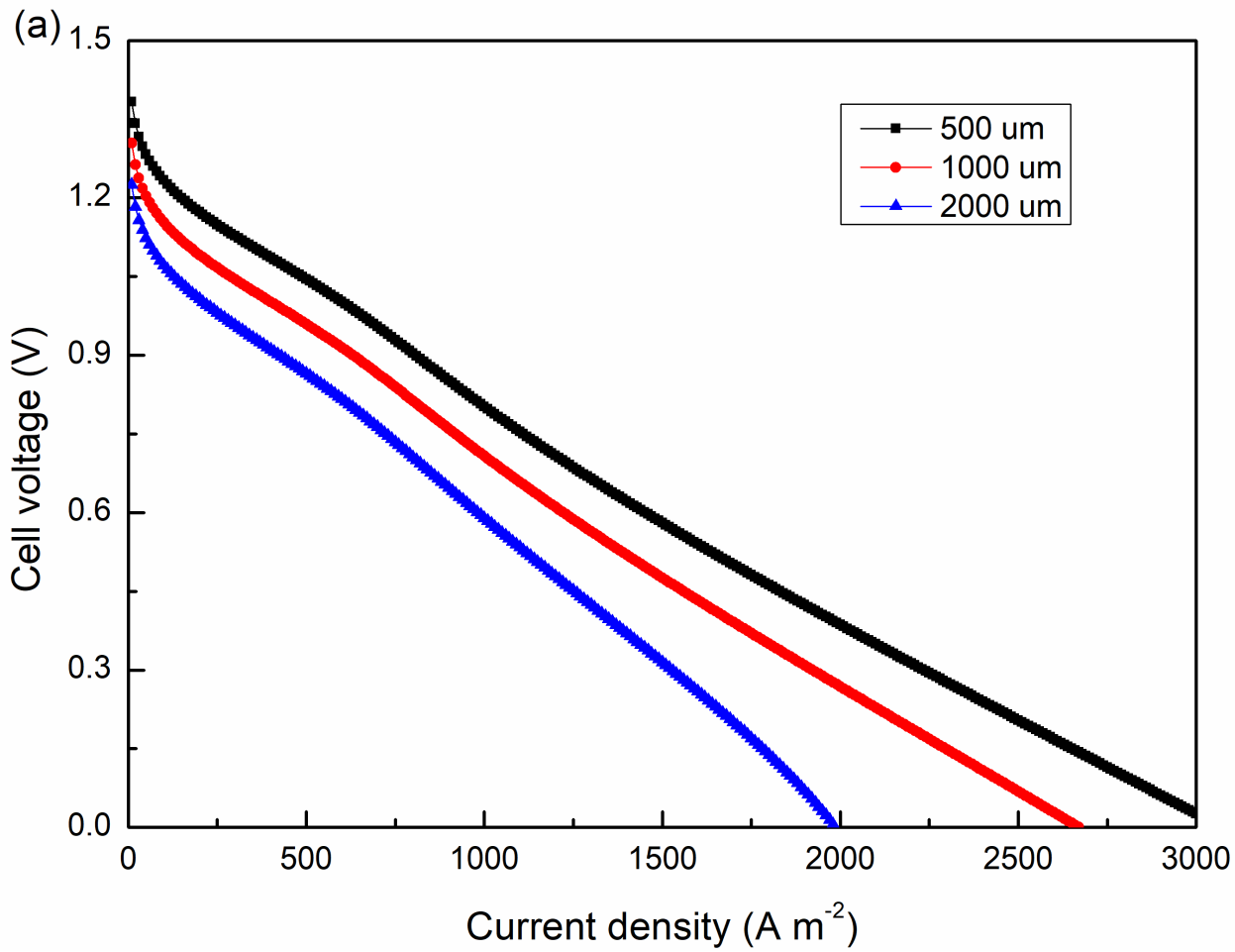
(a)
1.5
1.2
0.9
0.6
0.3
0.0
Cell voltage (V)
0
500
1000
1500
2000
2500
3000
Current density (A m-2)
500 um
1000 um
2000 um

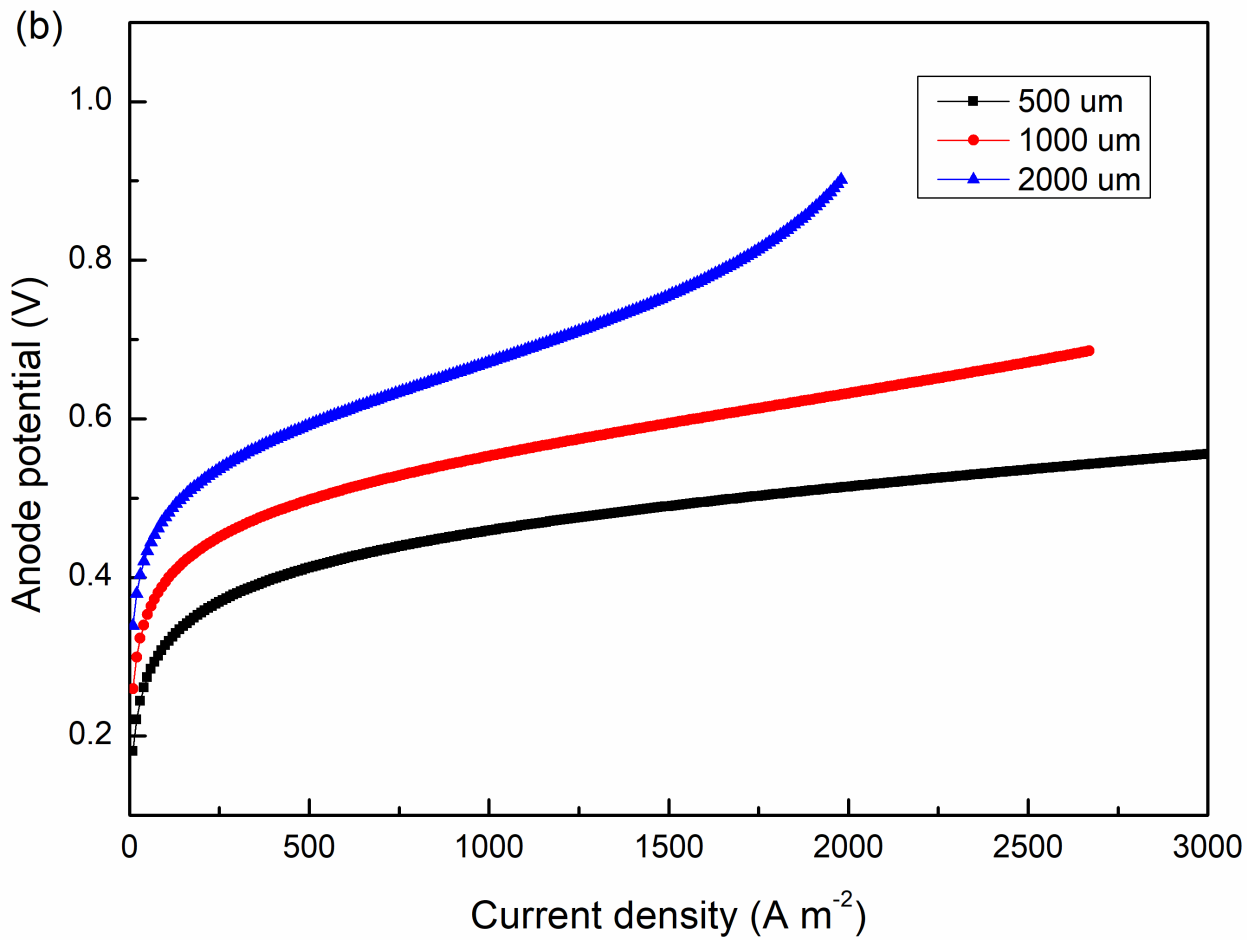


Figure 10 Effect of the anode DL thickness on the cell performance. (a) Polarization curves; and (b) Anode overpotentials.

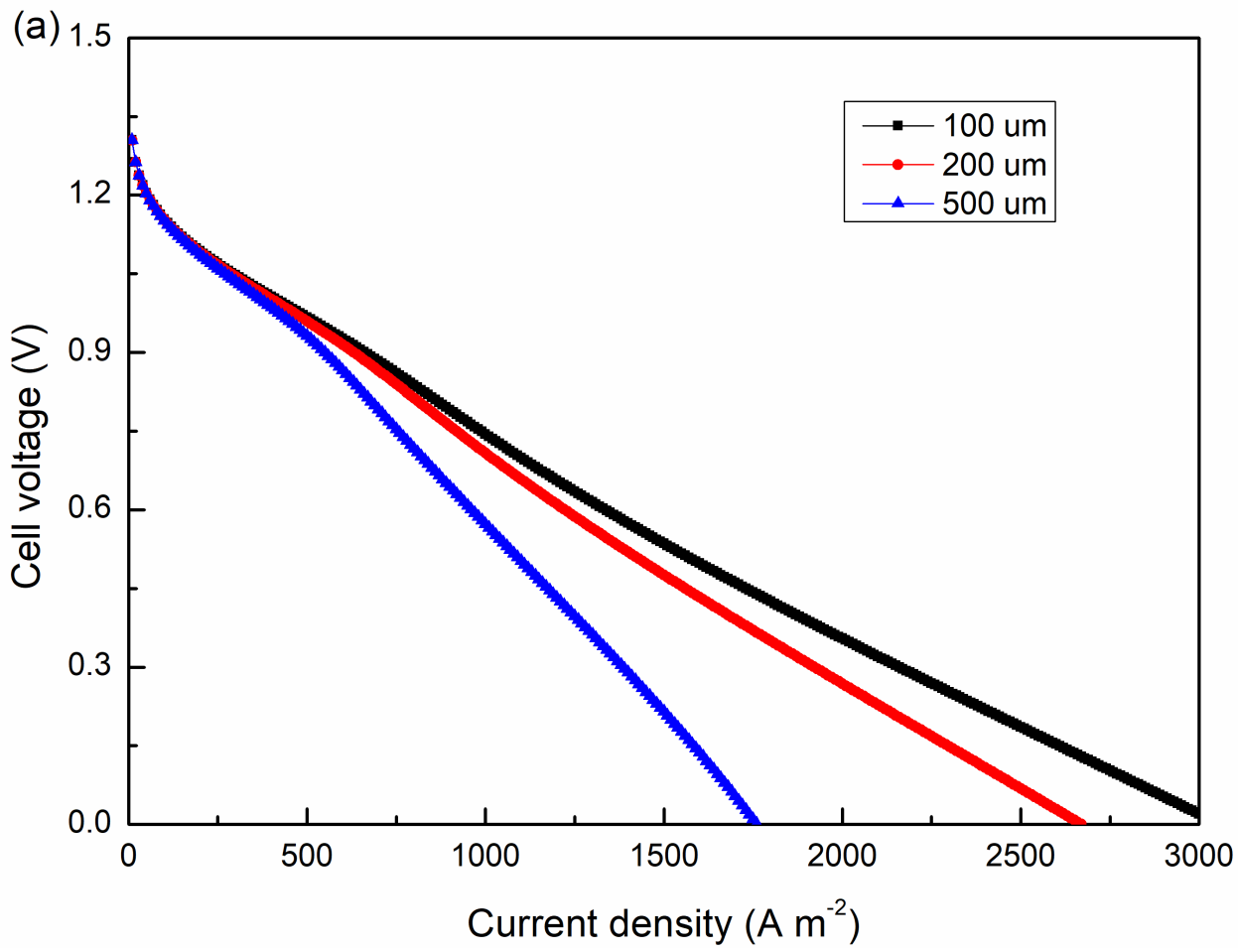
(a)
1.5
1.2
0.9
0.6
0.3
0.0
Cell voltage (V)
0
500
1000
1500
2000
2500
3000
Current density (A m-2)
100 um
200 um
500 um

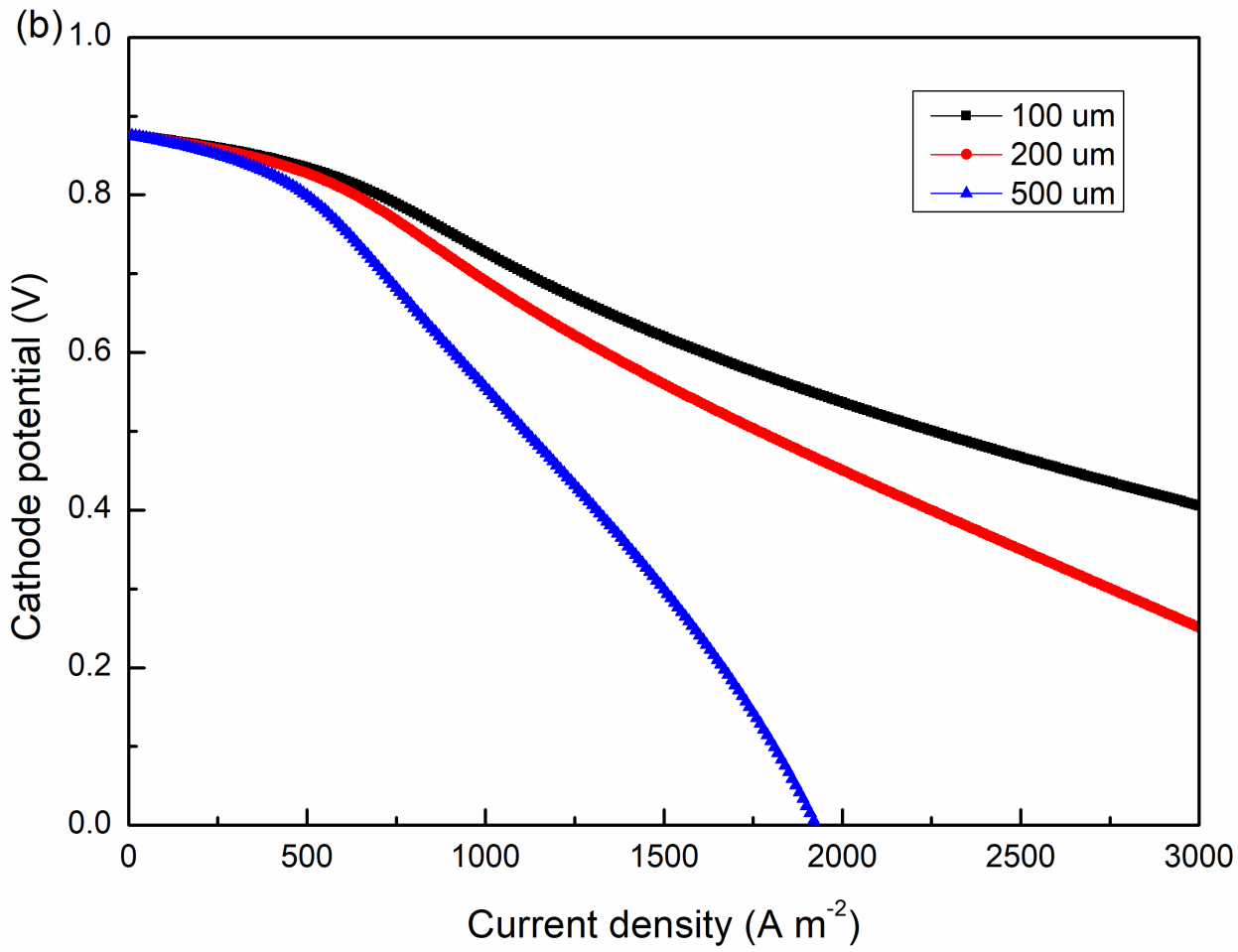


Figure 11 Effect of the cathode DL thickness on the cell performance. (a) Polarization curves; and (b) Cathode overpotentials.

| Table 1 – Physicochemical parameters | | | | |
|---|---|---|---|---|
| Parameter | Symbol | Value | Unit | Reference |
| Anode standard potential | $E_a^0$ | -0.69 | V | [11] |
| Anode transfer coefficient | $\alpha_a$ | 0.5 | - | Assumed |
| Anode exchange current density | $i_{0,a}$ | 10 | A $m^{-2}$ | Assumed |
| Number of anode transferred electrons | $n_a$ | 8 | - | |
| Hydraulic permeability | $k_w$ | $1.0\times10^{-14}$ | $m^2$ | [33] |
| Viscosity of water | $\mu_w$ | 0.000899 | Pa s | [33] |
| Pressure difference | $\Delta P$ | 1200 | Pa | [33] |
| Standard potential (HPRR) | $E_{HPRR}^0$ | 1.78 | V | [32] |
| Standard potential (HPOR) | $E_{HPOR}^0$ | 0.69 | V | [35] |
| Standard potential (ORR) | $E_{ORR}^0$ | 1.23 | V | [36] |
| Transfer coefficient (HPRR) | $\alpha_{HPRR}$ | 0.13 | - | Assumed |
| Transfer coefficient (HPOR) | $\alpha_{HPOR}$ | 0.9 | - | Assumed |
| Transfer coefficient (ORR) | $\alpha_{ORR}$ | 0.5 | - | [37] |
| Exchange current density (HPRR) | $i_{0,HPRR}$ | 10 | A $m^{-2}$ | [38] |
| Exchange current density (ORR) | $i_{0,ORR}$ | 44 | A $m^{-2}$ | [34] |
| Universal gas constant | $R$ | 8.314 | J $mol^{-1}$ $K^{-1}$ | |
| Faraday's constant | $F$ | 96485.3 | A s $mol^{-1}$ | |
| Number of transferred electrons (HPRR) | $n_{HPRR}$ | 2 | - | |
| Number of transferred electrons (HPOR) | $n_{HPOR}$ | 2 | - | |
| Number of transferred electrons (ORR) | $n_{ORR}$ | 4 | - | |
| Rate constant | $k_2$ | $1.01\times10^{-3}$ | mol $m^{-2}$ $s^{-1}$ | [39] |

| Table 2 – Operating parameters | | | | |
|---|---|---|---|---|
| Parameter | Symbol | Value | Unit | Reference |
| Operating temperature | $T$ | 333.15 | K | |
| Feeding concentration ($O_2$) | $C_{O_2}^F$ | 0 | mol $m^{-3}$ | Assumed |
| Reference concentration (EG) | $C_{EG}^{ref}$ | 1000 | mol $m^{-3}$ | Assumed |
| Reference concentration ($OH^-$) | $C_{OH^-}^{ref}$ | 7000 | mol $m^{-3}$ | Assumed |
| Reference concentration ($H_2O_2$) | $C_{H_2O_2}^{ref}$ | 4000 | mol $m^{-3}$ | [32] |
| Reference concentration ($H^+$) | $C_{H^+}^{ref}$ | 2000 | mol $m^{-3}$ | [32] |
| Reference concentration ($O_2$) | $C_{O_2}^{ref}$ | 36.573 | mol $m^{-3}$ | [34] |

| Table 3 – Structural parameters | | | | |
|---|---|---|---|---|
| Parameter | Symbol | Value | Unit | Reference |
| Anode DL porosity | $\varepsilon_{ADL}$ | 0.95 | - | [40] |
| Anode DL thickness | $l_{ADL}$ | $1.0\times10^{-3}$ | m | [40] |
| Anode CL porosity | $\varepsilon_{ACL}$ | 0.6 | - | [33] |
| Anode CL thickness | $l_{ACL}$ | $2.0\times10^{-5}$ | m | [33] |
| Anode CL bulk radius | $\delta_{ACL}$ | $2.0\times10^{-6}$ | m | [40] |
| Membrane thickness | $l_M$ | $5.0\times10^{-5}$ | m | Measured |
| Cathode DL porosity | $\varepsilon_{CDL}$ | 0.73 | - | [41] |
| Cathode DL thickness | $l_{CDL}$ | $2.0\times10^{-4}$ | m | [40] |

| Table 4 – Mass/charge transport parameters | | | | |
|---|---|---|---|---|
| Parameter | Symbol | Value | Unit | Reference |
| Diffusivity of $OH^-$ | $D_{OH^-}$ | $5.26\times10^{-9}$ | $m^2\ s^{-1}$ | [40] |
| Diffusivity of EG | $D_{EG}$ | $2.0\times10^{-9}$ | $m^2\ s^{-1}$ | [42] |
| Diffusivity of $H_2O_2$ | $D_{H_2O_2}$ | $3.47\times10^{-9}$ | $m^2\ s^{-1}$ | [43] |
| Diffusivity of $H^+$ | $D_{H^+}$ | $9.31\times10^{-9}$ | $m^2\ s^{-1}$ | [44] |
| Diffusivity of $O_2$ | $D_{O_2}$ | $3.03\times10^{-9}$ | $m^2\ s^{-1}$ | [45] |

**Nomenclature**

$C$
concentration (mol $m^{-3}$)

$D$
diffusivity ($m^2$ $s^{-1}$)

$E^0$
standard potential (V)

$E$
potential (V)

F
Faraday's constant (A s $mol^{-1}$)

$i_0$
exchange current density (A $m^{-2}$)

$j$
current density (A $m^{-2}$)

$K$
rate constant (mol $m^{-2}$ $s^{-1}$)

$k$
mass transfer coefficient (m $s^{-1}$)

$n$
number of electrons transferred

$N$
species flux (mol $m^2$ $s^{-1}$)

$R$
internal resistance (Ω)

$s$
stoichiometric coefficient

$V$
cell voltage (V)

$v$
superficial velocity (m $s^{-1}$)

Greek symbols

$\alpha$
transfer coefficient

$\varepsilon$
porosity of diffusion layer

$\delta$
bulk radius (m)

$\gamma$
reaction order

$\eta_a$
anode polarization (V)

$\eta_c$

cathode polarization (V)
$\theta_{H_2O_2}$
coverage of $H_2O_2$ on the catalyst

Subscripts and superscripts
a
anode
ADL
anode diffusion layer
ACL
anode catalyst layer
c
cathode
CCL
cathode catalyst layer
CDL
cathode diffusion layer
EGOR
ethylene glycol oxidation reaction
EG
ethylene glycol
eff
effective
F
feeding
HPRR
hydrogen peroxide reduction reaction
HPOR
hydrogen peroxide oxidation reaction
$H_2O_2$
hydrogen peroxide
$H^+$
proton
i
different species
M
membrane
w
water
$OH^-$
hydroxyl ion
ORR
oxygen reduction reaction
$O_2$
oxygen
ref

reference
R
reactant
S
catalyst surface